Journal of Energy Storage 65 (2023) 107233

Contents lists available at ScienceDirect

Journal of Energy Storage

journal homepage: www.elsevier.com/locate/est

Research papers

Laminar forced convection in a tube with a nano-encapsulated phase change materials: Minimizing exergy losses and maximizing the heat transfer rate

Ehsan Golab [a,b], Behzad Vahedi [b], Ankur Jain [c], Robert A. Taylor [d], Kambiz Vafai [e,*]

[a] Department of Mechanical Engineering, Sharif University of Technology (SUT), Tehran, Iran
[b] Functional Neurosurgery Research Center, Shohada Tajrish Comprehensive Neurosurgical Center of Excellence, Shahid Beheshti University of Medical Sciences, Tehran, Iran
[c] Department of Mechanical and Aerospace Engineering, The University of Texas at Arlington, Arlington, TX, USA
[d] School of Mechanical and Manufacturing Engineering, University of New South Wales, Sydney 2052, Australia
[e] Mechanical Engineering Department, University of California, Riverside, CA 92521, United States of America

ARTICLE INFO

Keywords:
Nano-encapsulated phase change material
Forced convection
Exergy analysis
Latent heat energy storage
Energy storage materials
Nanofluid

ABSTRACT

The present work investigates the potential of NEPCM mixtures via analyses of convective heat transfer and exergy losses, and trade-offs between them inside a tube with a constant wall temperature. Experimental data for viscosity and thermal conductivity of the mixture was used within numerical simulations over a broad range of dimensionless parameters, including Reynolds number, mass fraction, melting strength, phase change zone thickness, and location of phase change zone. The effect of these parameters on the melting process, convective heat transfer and exergy loss is evaluated. The findings indicate that, although employing a NEPCM can boost the Nusselt number and heat transfer rate by 9.3 % and 16.1 %, as compared to the water, the exergy losses were enhanced up to 17 %. Additionally, in some circumstances, the Nusselt number and heat transfer rate both increased by 5.9 % and 2.5 %, respectively, whereas the exergy losses were zero. An optimal value of $\omega = 0.02$ was found to provide reasonable improvement in heat transfer rate increase with no exergy losses. Importantly, the present study shows that although higher NEPCM mass fractions can continue to increase the heat transfer performance, their benefit is rapidly offset above $\omega = 0.02$ due to heat transfer related exergy losses. Additionally, it was concluded that, in comparison to other parameters, the location of the phase change and the mass concentration of NEPCMS substantially affected the percentage of molten NEPCM and the latent heat efficacy.

1. Introduction

Most heat transfer processes utilize a circulating working fluid, wherein the aim is to efficiently transfer heat from one component to another. This type of process necessitates some entropy generation due to the presence of fluid friction and a temperature gradient (i.e., the thermodynamic quality of the transferred heat goes down) [1]. Entropy and exergy analysis of energy transfer processes is a key theoretical tool for understanding and optimizing rates of heat transfer, efficiency and other thermal performance parameters. The system design, fluid properties, and flow characteristics all influence the extent of entropy generation [2]. To gauge the full irreversibility or exergy losses of the system, we must also consider the effects of ambient temperature of the working system [3,4]. To understand and improve heat transfer systems, numerous researchers have carried out exergy analyses for forced convection inside tubes and channels [5–8]. In many recent studies, various nanoparticles have been incorporated into these conventional systems, targeting an overall improvement in exegetic efficiency. For example, Vahedi et al. [9] numerically simulated nanofluid flow in a parabolic trough collector absorber tube to calculate the exergy losses involved in both laminar and turbulent forced convection flows. Their findings indicated that nanofluids reduced the temperature gradient in the fluid due to their higher thermal conductivity, causing less exergy destruction relative to pure synthetic pure oil. However, an overall exergy improvement is not always guaranteed by blindly adding nanomaterials to a working fluid, even if there is a positive change in the thermal properties of the base fluid [10,11]. This is because the addition of particles also makes the base fluid more viscous, so care must be taken to choose an appropriate mass fraction. When compared to other heat

* Corresponding author.
E-mail address: vafai@engr.ucr.edu (K. Vafai).

https://doi.org/10.1016/j.est.2023.107233
Received 11 December 2022; Received in revised form 10 March 2023; Accepted 22 March 2023
Available online 5 April 2023

Nomenclature

C_P	Specific heat capacity, [J kg^{-1} K^{-1}]
$C_{P,cl}$	Specific heat capacity of core in liquid phase, [J kg^{-1} K^{-1}]
$C_{P,n}$	Specific heat capacity of NEPCM, [J kg^{-1} K^{-1}]
$C_{P,c}$	Specific heat capacity of core, [J kg^{-1} K^{-1}]
$f(\theta)$	Melting function
h	Convective heat transfer, [W m^{-2} K^{-1}]
h_{sf}	Latent heat of core, [J kg^{-1}]
k	Thermal conductivity, [W m^{-1} K^{-1}]
L	Length of the Tube, [m]
P	Pressure, [N m^{-2}]
$\dot{Q}_{latent}$	Received latent heat, [W]
$\dot{Q}_{tot}$	Received total heat, [W]
T	Temperature, [K]
T_{Mr}	Melting range of core, [K]
$\dot{m}$	Mass flow rate, [kg s^{-1}]
T_F	Fusion temperature, [K]
V	Velocity vector, [m/s]
r, θ, z	Cylindrical coordinate, [m]
X	Exergy losses, [W]

Dimensionless numbers

Br	Brinkman number
C_r	Heat capacity ratio of the mixture to base fluid
Nu	Nusselt number
Pe	Peclet number
Pr	Prandtl number
St	Stefan number
Re	Reynolds number
λ	Heat capacity ratio of the NEPCM particles to base fluid
χ	Melting strength
δ	Phase change zone's thickness
θ_f	Location of phase change zone
θ	Dimensionless Temperature

Greek letters

α	Thermal diffusivity, [m^2 s^{-1}]
β	Core-shell weight ratio, [−]
ω	Mass fraction, [−]
μ	Dynamic viscosity, [kg m^{-1} s^{-1}]
ν	kinematic viscosity, [m^2 s^{-1}]

Subscripts

C	Cold
Ave	Average
b	Bulk
c	Core
D	Diameter
H	Hot
HT	Heat transfer
In	Inlet
W	Water
r	Ratio
f	fluid
m	Mixture
Loc	Local
bf	Base fluid
W	Wall
nf	Nanofluid
Var	Variation

Table 1
Recent studies related to heat transfer enhancement with NEPCM/MEPCM.

Studies and experimental/ numerical	NEPCM/ MEPCM	Heat transfer mechanism and regime of flow	Geometry	Concentration	Result
Zhang et al. [29] *Exp*	*MEPCM*	Forced convection & turbulent	Circular tube	5 wt%	Nusselt number was increased by 25 %
Lu et al. [30] *Num*	*NEPCM*	Forced convection & laminar	Rectangular Duct	30 wt%	Heat transfer rate was promoted by 19 %
Golab et al. [31] *Num*	*NEPCM*	Natural convection	Rectangular cavity	3.5 wt%	Heat transfer was enhanced by 33 %
Moshtagh et al. [32] *Num and exp*	*MEPCM*	Forced convection & laminar	Tube	15 wt%	Heat transfer was improved by 38.9 %
Sabbah et al. [33] *Exp*	*MEPCM*	Forced convection & laminar	Tube	20 wt%	Heat transfer was enhanced by 45 %
Kong et al. [34] *Exp*	*MEPCM*	Forced convection & turbulent	Coil heat exchangers	7.4 wt%	Heat transfer was enhanced by 17 %

transfer enhancement mechanisms (i.e., porous media, extended surfaces, and vortex generators [12–16]), it can be inferred that almost all heat transfer enhancement schemes eventually give rise to fluid friction (and associated entropy generation). Sureshkumar et al. [17] reviewed the impacts of adding nanoparticles into the conventional working fluids in heat pipes and corroborated that it is possible to boost the thermal efficiency of phase change systems, likely due to the mixture's thermal conductivity enhancement. Here again, if nanoparticle loading becomes high, the performance degrades. It has also been shown that the use of nanoparticles in liquid-to-vapor phase change fluids can not only make systems more compact but change boiling/condensation heat transfer rates (e.g., [18,19]).

Solid-liquid phase change can approach a reversible process, with no entropy generation, particularly when there is little buoyant force and volume expansion in phase transition [20]. It is noteworthy that liquid-solid phase transition involves much lower volume change than solid-gas and liquid-gas phases transitions. Therefore, PCMs have been widely used for solar water heaters [21], thermal management of electronic devices [22], thermal management system [23], and cooling process [24]. The two main issues associated with using PCMs are their low thermal conductivity and high viscosity. Several novel techniques have been investigated to mitigate these problems. Mostafavi et al. [25] have theoretically investigated the use of PCM and fins in a cylindrical phase change energy storage equipment to observe the impacts of extended surfaces as a thermal conductivity booster on heat transfer. Ghahremannezhad et al. [26] simulated a latent heat energy storage system and heat sinks, comprised of a gradient porous media and PCM. Their findings indicated that embedding a non-homogenous porous

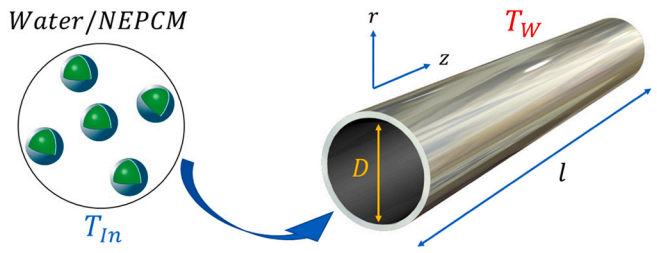

Fig. 1. Physical model including a tube and water-NEPCM mixture.

Table 2
The boundary conditions of the present study.

Patch	Velocity	Temperature	Pressure
Inlet	$V_r = V_{in}\left[1-4\left(\frac{r}{D}\right)^2\right], V_z = 0$	$T = T_{in}$	$\frac{\partial p}{\partial z} = 0$
Wall	$V_r = V_z = 0$	$T = T_W$	$\frac{\partial p}{\partial z} = 0$
Outlet	$\frac{\partial V_r}{\partial z} = \frac{\partial V_z}{\partial z} = 0$	$\frac{\partial T}{\partial z} = 0$	$p = 0$

media had a crucial role in providing a better and uniformed melting profile since it acts as a thermal conductivity enhancer. Moreover, to make PCMs a pumpable fluid and alleviate their high viscosity, it has been proposed that they be incorporated in the form of suspended encapsulations of micro/nano-sized particles (MEPCM/NEPCM) [27]. By adding MEPCM/NEPCM to a working fluid, it is plausible to take advantage of the solid-liquid phase transition process. This type of fluid may store heat through two mechanisms: the global temperature of the mixture (sensible heat) and the freezing/melting of the PCM additives (latent heat) [28]. The inclusion of encapsulated phase change materials into base fluid has shown significant potential for heat transfer performance improvement. Table 1 summarizes key recent literature in this direction.

Although using NEPCMs have some limitations, their superiority over MEPCMs are not neglectable. The results indicated that the larger the size of capsules inside the system, the slower the melting process. Consequently, it can be claimed that using NEPCM alleviates the duration of the phase change process [35]. Moreover, it should be emphasized that since the phase change duration of NEPCMs is shorter than the MEPCMs in solidification, the likelihood of moving closer to each other or moving downward is lower [36]. In other words, NEPCMs have a lower chance of being clustered and sedimented in comparison to MEPCMs in the same period of working time [37]. Therefore, the detrimental consequences and chances of collision in MEPCMs are much higher than NEPCMs, leading to erosion, particle deformation, and pump damage [38–40].

As can be seen in Table 1, most of the studies have focused on the potential of NEPCM/MEPCM for improvement in heat transfer characteristics of a thermal system. However, the literature does not sufficiently address exergy destruction associated with the use of NEPCM/MEPCM. There is no past work on understanding and optimizing the trade-offs between heat transfer enhancement and exergy losses. As such, the present study aims to conduct the first investigation to minimize exergy losses and maximize the heat transfer rate based by showing that minimizing exergy losses and maximizing the heat transfer rate depends on a combination of the following key dimensionless parameters: melting strength (MS), thickness (TPCZ) and location of phase change zone (LPCZ), mass fraction and Reynolds number. In addition, the impact of these parameters on the percentage of molten NEPCM at the outlet and latent heat efficiency is investigated. It is expected that through simultaneous analysis of exergy losses and heat transfer, it will be possible to gain valuable insights into the underlying NEPCM melting process and to pave the way for researchers to fine-tune NEPCM/MEPCM systems to their specific application.

The rest of the paper is organized as follows: Section 2 describes the physical model for this problem. Section 3 describes the mathematical model in detail, including conservation equations and boundary conditions. The numerical methodology is discussed in Section 4, followed by discussion of validation exercises in Section 5. Key results are presented in Section 6, followed by concluding remarks in Section 7.

2. Description of physical model

As shown in Fig. 1, a mixture of water and nano-encapsulated phase change material with inlet temperature T_{in} and axial velocity $V_{in}(r)$ enters a hollow tube with diameter D and length L. The NEPCM considered here comprises of n-eicosane and Sodium Lauryl Sulphate (SLS) as core and shell, respectively, both of which are commonly used materials. In the current study, the mass ratio of core to shell was held constant at 0.25, and the latent heat of n-eicosane was 247 $kJ{\cdot}kg^{-1}$. In addition, the melting temperature was 37°C over a 2°C range.

Fig. 1 shows green spherical particles, which represent the NEPCM particles. The mixture is homogeneous and the NEPCM is completely in solid phase at the entrance of the tube. Moreover, the NEPCM at the entrance was completely in solid phase. Some of the wall heat is used to melt the NEPCM core, while the rest increases the temperature of the mixture. Note that to observe the impact of phase change on heat transfer process, the mixture temperature must be close to the melting temperature range of the NEPCM core. Therefore, correct selection of the flow characteristics (including fluid velocity, geometry, and boundary conditions), the base fluid (thermal properties), and the type of NEPCM core (melting temperature and latent heat) all play a critical role in the effectiveness of the heat transfer process.

3. Mathematical formulation

3.1. Governing equations and boundary conditions

Several assumptions were made in order to simplify the analysis of forced convection heat transfer of the water-NEPCM mixture inside the tube. Flow is assumed to be steady and incompressible, and the effect of dissipation was neglected due to low Brinkman number. Moreover, the mixture is assumed to be homogeneous, with no changes in NEPCM material properties during phase change, except for the heat capacity [41]. Since the Biot number is $<< 0.1$ for nanoparticles with a characteristic length of 1–100 $\times$ 10^{-9} m, the NEPCMs were assumed to have a lumped-capacitance characteristic in the simulations. Moreover, since modeling of individual NEPCM in the flow is computationally very intensive for large numbers of NEPCM particles (e.g., via molecular dynamics [42] or Lattice Boltzmann [43] simulations), this study employs continuum conservation equations and accounts for the NEPCMs through effective mixture properties (see Eqs. (8) and (9)). So, the NEPCMs were considered using a lumped approach. Deformation of NEPCMs during phase change process was neglected in this study, as suggested in reference [41]. The dimensional form of mass, momentum, and energy conservation equations in cylindrical coordinates may be written as in reference [44]:

$$\frac{1}{r}\frac{\partial}{\partial r}(rV_r) + \frac{\partial V_z}{\partial z} = 0 \tag{1}$$

$$\rho_m\left(V_r\frac{\partial V_r}{\partial r} + V_z\frac{\partial V_r}{\partial z}\right) = -\frac{\partial p}{\partial r} + \mu_m\left(\frac{\partial^2 V_r}{\partial r^2} + \frac{1}{r}\frac{\partial V_r}{\partial r} - \frac{V_r}{r^2} + \frac{\partial^2 V_r}{\partial z^2}\right) \tag{2}$$

$$\rho_m\left(V_r\frac{\partial V_z}{\partial r} + V_z\frac{\partial V_z}{\partial z}\right) = -\frac{\partial p}{\partial z} + \mu_m\left(\frac{\partial^2 V_z}{\partial r^2} + \frac{1}{r}\frac{\partial V_z}{\partial r} + \frac{\partial^2 V_z}{\partial z^2}\right) \tag{3}$$

$$V_r\frac{\partial}{\partial r}(\rho_m C_{p,m}T) + V_z\frac{\partial}{\partial z}(\rho_m C_{p,m}T) = k_m\left(\frac{1}{r}\frac{\partial}{\partial r}\left(r\frac{\partial T}{\partial r}\right) + \frac{\partial^2 T}{\partial z^2}\right) \tag{4}$$

Table 3
Thermophysical properties of water, n-eicosane, and SLS at 25°C [48].

Material	$\rho\left(\frac{kg}{m^3}\right)$	$C_p\left(\frac{J}{kgK}\right)$	$k\left(\frac{W}{mK}\right)$	$\mu\times10^{-6}\left(\frac{kg}{ms}\right)$
Water	995	4200	0.63	700
n-Eicosane	780	2460	–	–
SLS	1050	1300	–	–

Table 4
Density, dynamic viscosity, and thermal conductivity of mixture (water/n-eicosane-SLS) in T = 25°C [48].

Mass fraction (ω)	Volume fraction (φ)	$k_m\left(\frac{W}{mK}\right)$	$\mu_m\left(\frac{kg}{ms}\right)$	$\rho_m\left(\frac{kg}{m^3}\right)$
0.01	0.0121	0.68	0.8×10^{-3}	994
0.02	0.0241	0.61	0.87×10^{-3}	992
0.05	0.0598	0.66	1.1×10^{-3}	985

At the inlet, the flow was presumed to be hydrodynamically fully developed, so that the laminar velocity profile of the HTF flow was parabolic. Also at the inlet, the temperature (T_{in}) was constant and no pressure gradient was present. At the wall, the no-slip condition was used, so the velocity would be zero. The tube wall temperature was kept at a uniform, constant value of $T_W > T_{in}$. At the outlet, a zero temperature and velocity gradient and zero pressure boundary condition was assumed, along with fully developed flow. The dimensional form of these boundary conditions are summarized in Table 2.

3.2. Mixture properties

The density and heat capacity ratio properties of NEPCM are a function of shell and core properties. It should be noted that the latent heat due to phase change affects heat capacity of core leading to obey a sinusoidal function that can be represented as below [45,46]:

$$\rho_n = \frac{(1+\beta)\rho_c\rho_s}{\rho_s+\beta\rho_c} \tag{5}$$

$$C_{p,c} = C_{p,cl} + \left\{\frac{\pi}{2}\left(\frac{h_{sf}}{T_{Mr}} - C_{p,c\,l}\right)\left(sin\pi\frac{T-(T_f-T_{Mr}/2)}{T_{Mr}}\right)\right\}\times\begin{cases}0\ if\ T<T_f-\frac{T_{Mr}}{2}\\ 1\ if\ T_f-\frac{T_{Mr}}{2}<T<T_f+\frac{T_{Mr}}{2}\\ 0\ if\ T<T_f+\frac{T_{Mr}}{2}\end{cases} \tag{6}$$

$$C_{p,n} = \frac{(C_{p,c}+\beta C_s)\rho_c\rho_s}{(\rho_s+\beta\rho_c)\rho_n} \tag{7}$$

It should be noted that the effects of specific heat capacity of NEPCM's core in the liquid or solid phase and its latent heat have been analyzed by Alisetti and Roy [47]. $\beta, C_{p,cl}, h_{sf}, T_{Mr}$, and T_f refer to mass ratio of core to shell, specific heat capacity of *n-eicosane* in liquid phase, latent heat of core in solid to liquid phase transition, melting range of *n-eicosane*, and the melting point, respectively. Values of key thermal properties of materials were taken from past and were summarized in Table 3. Note that the viscosity and thermal conductivity of the present study are extracted from an experimental study [48] instead of calculating the mixture properties using each of the base fluid and NEPCM properties.

Table 5
The non-dimensional form of boundary conditions.

Name of boundary	Velocity	Temperature	Pressure
Inlet	$V_R = 1-4R^2, V_Z = 0$	$\theta = 0$	$\frac{\partial P}{\partial z} = 0$
Wall	$V_R = V_Z = 0$	$\theta = 1$	$\frac{\partial P}{\partial z} = 0$
Outlet	$\frac{\partial V_R}{\partial Z} = \frac{\partial V_Z}{\partial Z} = 0$	$\frac{\partial \theta}{\partial Z} = 0$	$P = 0$

Table 6
Values of various property ratios of mixture to base fluid.

ω	φ	$\frac{\rho_m}{\rho_f}$	$\frac{\mu_m}{\mu_f}$	$\frac{k_m}{k_f}$
0	0	1	1	1
0.01	0.0121	0.998	1.143	1.079
0.02	0.0241	0.996	1.243	0.968
0.05	0.0598	0.990	1.571	1.048

Further, the effective density and heat capacity of the fluid flow were given by the following mixture rules [11]:

$$\rho_m = (1-\varphi)\rho_{bf} + \varphi\rho_n \tag{8}$$

$$C_{P,m} = \frac{(1-\varphi)\rho_f C_{P,f} + \varphi\rho_n C_{P,n}}{\rho_m} \tag{9}$$

The density, dynamic viscosity, and thermal conductivity of the mixture are derived from experimental results [48] that used the same core and shell materials as the present work. These values are listed in Table 4.

Finally, the mass fraction and volume fraction were related to each other as follows [48]:

$$\varphi = \left(\frac{(1-\omega)\rho_n}{\rho_f\omega} + 1\right)^{-1} \tag{10}$$

3.3. Non-dimensionalization

The following scheme for non-dimensionalization was used:

$$R = \frac{r}{D}, Z = \frac{z}{D}, L = \frac{l}{D}, V_R = \frac{V_r}{V_{In}}, V_Z = \frac{V_z}{V_{In}}, P = \frac{p}{\rho_f {V_{In}}^2}, \theta = \frac{T-T_{in}}{\Delta T}, \Delta T = T_W - T_{In} \tag{11}$$

Non-dimensionalized kinematic viscosity $\nu_f = \frac{\mu_f}{\rho_f}$, thermal diffusivity $\alpha_f = \frac{k_f}{(\rho c_p)_f}$, Reynolds number $Re_f = \frac{V_{In}D}{\nu_f}$ and Prandtl number $Pr_f = \frac{\nu_f}{\alpha_f}$ appear in the governing equations and boundary conditions as follows [49]:

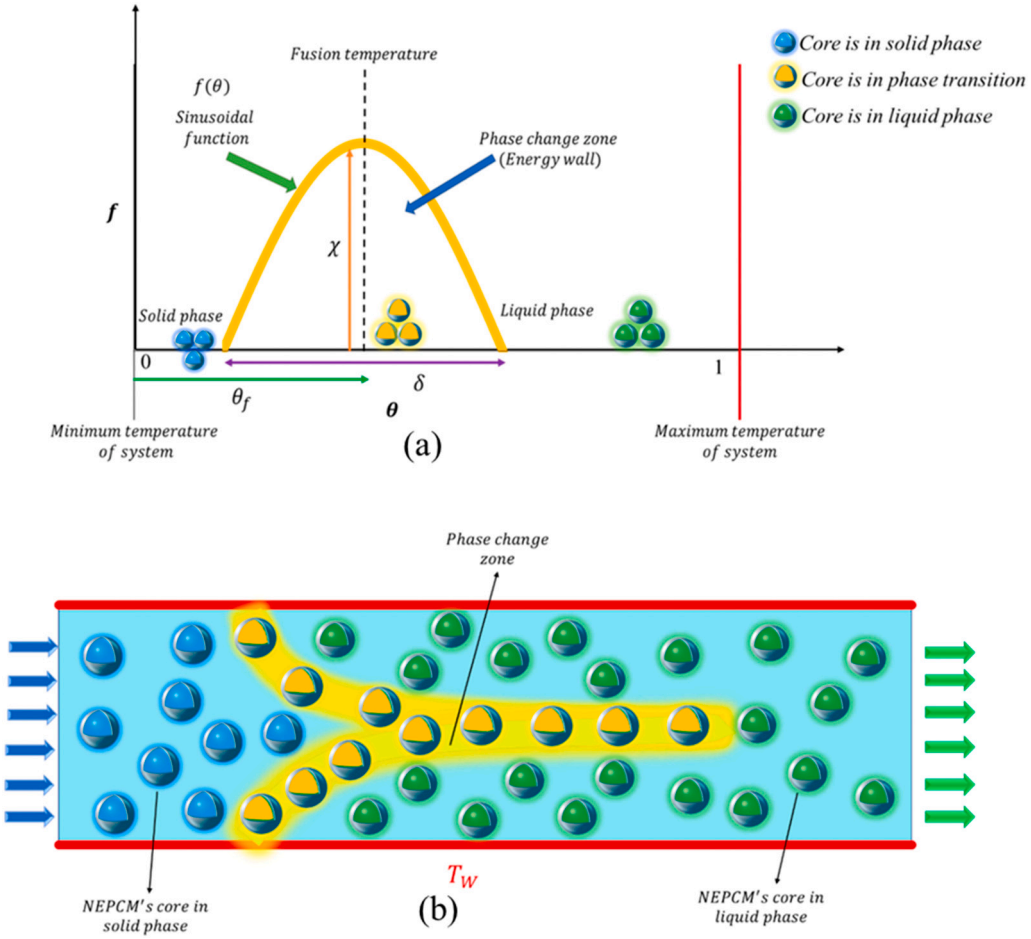

Fig. 2. (a) The illustration of phase change zone (energy wall [31]) with its details and (b) the behavior of NEPCMs in melting process for forced convection flow in a circular tube.

$$\frac{1}{R}\frac{\partial}{\partial R}(RV_R)+\frac{\partial V_Z}{\partial Z}=0 \tag{12}$$

$$\left(\frac{\rho_m}{\rho_f}\right)\left(V_R\frac{\partial V_R}{\partial R}+V_Z\frac{\partial V_R}{\partial Z}\right)=-\frac{\partial P}{\partial R}+\frac{1}{Re_f}\left(\frac{\mu_m}{\mu_f}\right)\left(\frac{\partial^2 V_R}{\partial R^2}+\frac{1}{R}\frac{\partial V_R}{\partial R}-\frac{V_R}{R^2}+\frac{\partial^2 V_R}{\partial Z^2}\right) \tag{13}$$

$$\left(\frac{\rho_m}{\rho_f}\right)\left(V_R\frac{\partial V_Z}{\partial R}+V_Z\frac{\partial V_Z}{\partial Z}\right)=-\frac{\partial P}{\partial Z}+\frac{1}{Re_f}\left(\frac{\mu_m}{\mu_f}\right)\left(\frac{\partial^2 V_Z}{\partial R^2}+\frac{1}{R}\frac{\partial V_Z}{\partial R}+\frac{\partial^2 V_Z}{\partial Z^2}\right) \tag{14}$$

$$V_R\frac{\partial}{\partial R}(C_r\theta)+V_Z\frac{\partial}{\partial Z}(C_r\theta)=\frac{1}{Pr_f Re_f}\left(\frac{k_m}{k_f}\right)\left(\frac{1}{R}\frac{\partial}{\partial R}\left(R\frac{\partial\theta}{\partial R}\right)+\frac{\partial^2\theta}{\partial Z^2}\right) \tag{15}$$

where V_R, V_Z, P and θ denote dimensionless velocity in R and Z directions, pressure, and temperature, respectively. Moreover, μ, ρ, k, and C_r represent dynamic viscosity, density, thermal conductivity, and heat capacity ratio of mixture to base fluid, respectively. The non-dimensional form of boundary conditions for velocity and temperature are listed in Table 5. Using information summarized in Table 2, the values of various property ratios are listed in Table 6. Also, C_r depends on a sinusoidal function of melting function ($f(\theta)$) and various parameters, which can be calculated as below [49]:

$$C_r=\frac{\rho_m C_{p,m}}{\rho_f C_{p,f}}=1+(f(\theta)+\lambda-1)\varphi \tag{16}$$

where λ and φ are the ratio of heat capacities of the NEPCM particles and base fluid, and volume fraction of NEPCM, respectively. The various non-dimensional parameters appearing in Eq. (16) can be expressed as [49]:

$$\lambda=\frac{(C_{p,cl}+\beta C_s)\rho_c\rho_s}{(\rho_s+\beta\rho_c)(\rho C_P)_f} \tag{17}$$

$$\chi=\frac{1}{\delta\times Ste}=\frac{h_{sf}/T_{Mr}}{C_{P,f}}\frac{(\rho_s\rho_c)}{\rho_f(\rho_s+\beta\rho_c)} \tag{18}$$

$$\delta=\frac{T_{Mr}}{T_W-T_{In}} \tag{19}$$

$$\theta_f=\frac{T_f-T_{In}}{T_W-T_{In}} \tag{20}$$

Using Eq. (6), the non-dimensional melting function is defined as:

$$f(\theta)=\chi\,\frac{\pi}{2}sin\frac{\pi}{\delta}\left(\theta-\theta_f+\frac{\delta}{2}\right)\times\begin{cases}0\ if\ \theta<\theta_f-\dfrac{\delta}{2}\\ 1\ if\ \theta_f-\dfrac{\delta}{2}<\theta<\theta_f+\dfrac{\delta}{2}\\ 0\ if\ \theta<\theta_f+\dfrac{\delta}{2}\end{cases} \tag{21}$$

The dimensionless Eqs. (17) to (21) can be used to systematically study the effects of $V_{in}, \Delta T, h_{sf}$ and T_{In}, as well as non-dimensional parameters such as Re, δ, χ and θ_f.

A key output parameter in convective heat transfer analysis is the average Nusselt number that represents the average convective heat

Table 7
Grid independence: average Nusselt number computed with different number of nodes in R and Z directions.

Node number (Z × R)	Nu_{Ave}	Relative difference%	Node number (Z × R)	Nu_{Ave}	Relative difference%
200 × 20	11.981	1.57	300 × 20	11.971	1.45
200 × 30	11.823	0.25	300 × 30	11.863	0.25
200 × 40	11.808	0.12	300 × 40	11.846	0.1
200 × 50	11.801	0.07	300 × 50	11.838*	0.03
200 × 60	11.793	*Reference*	300 × 60	11.834	*Reference*
250 × 20	11.976	1.36	350 × 20	11.961	1.05
250 × 30	11.843	0.25	350 × 30	11.887	0.44
250 × 40	11.827	0.11	350 × 40	11.858	0.19
250 × 50	11.819	0.05	350 × 50	11.837	0.02
250 × 60	11.813	*Reference*	350 × 60	11.835	*Reference*

transfer between the pipe and fluid. The average Nusselt number was determined as follows:

$$Nu_{Ave} = \frac{D}{k_m}\frac{1}{L}\int_0^L \frac{k_m}{T_W - T_b(z)}\left(\frac{\partial T}{\partial r}\right)_{r=D/2} dz \tag{22}$$

where $T_b(z)$ was the volume-averaged bulk temperature given by

$$T_b = \frac{\int (\rho C_P)_{m0} T\vec{V} \bullet d\vec{A}}{\int (\rho C_P)_{m0} \vec{V} \bullet d\vec{A}} \tag{23}$$

Table 8
The average Nusselt number of present study and Zeinali et al. [57] for $\varphi_{Al_2O_3} = 0.02$.

Pe	Experimental. Zeinali [57]	Numerical. Present study	Error (%)
2500	5.13	4.91	4.3
3500	6.04	5.74	4.9
4500	6.8	6.43	5.4
5500	7.4	7.07	4.4

where $d\vec{A} = 2\pi r dr\ \vec{n}$ and $\vec{n}$ is a vector perpendicular to the cross-section area.

In this study, the NEPCM's phase change was a sinusoidal function within a base fluid (see Fig. 2(a)). Golab et al. [31] proposed the concept of energy wall (or phase change zone) to model the behavior of NEPCM in a fluid (see Fig. 2(a)). The phase change zone is characterized by melting strength (χ), thickness (δ), and location (θ_f) as follows:

$$f(\theta) = \chi\ \frac{\pi}{2} sin\frac{\pi}{\delta}\left(\theta - \theta_f + \frac{\delta}{2}\right) \tag{24}$$

where χ means the ratio of latent to sensible heat of NEPCM, δ is the ratio of melting temperature range to temperature difference (minimum and maximum temperature of system), and θ_f is the distance of phase change zone relative to minimum temperature. If $\theta_f > 0$, all the NEPCM core that enters the tube is in solid phase. Conversely, if $\theta_f < 0$, then all of the NEPCM core that enters the tube was in liquid phase.

Fig. 2(b) concisely sheds light on the melting process of NEPCM core during flow in a tube with constant temperature wall. Three distinct

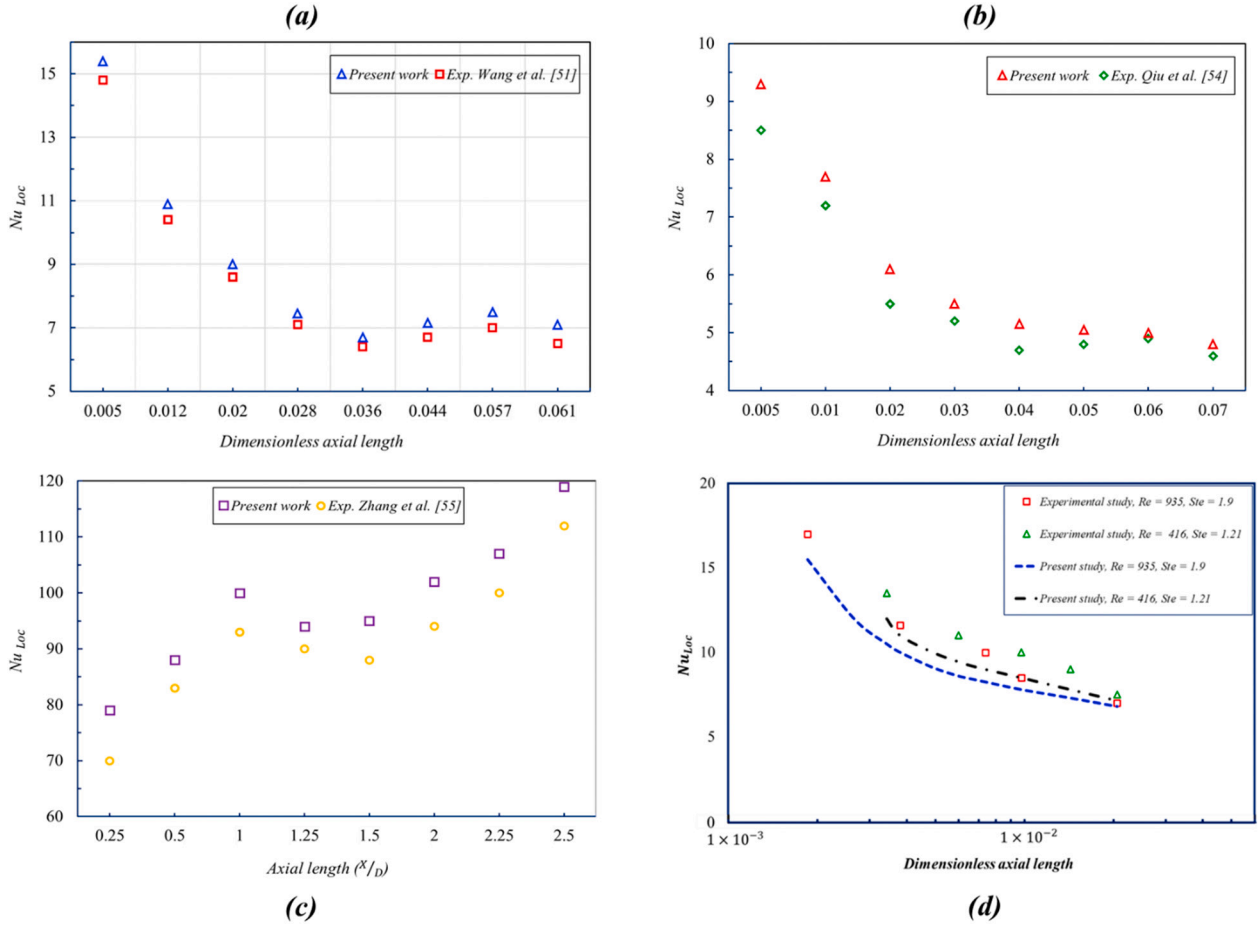

Fig. 3. Comparison between the present numerical study for Nu_{Loc} and the experimental studies of (a) Wang et al. [53], (b) Qiu et al. [54], (c) Zhang et al. [55], and (d) Chen et al. [56].

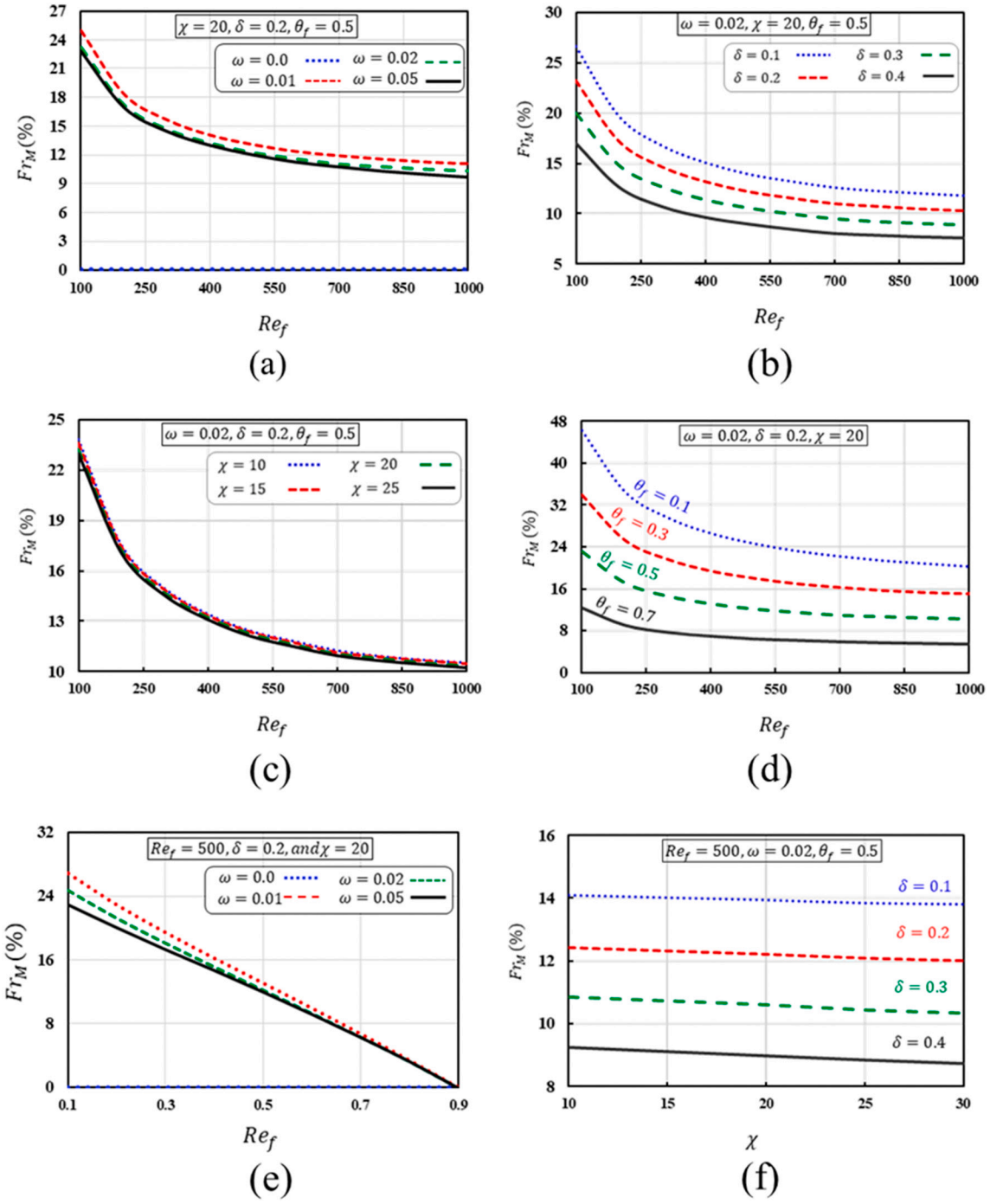

Fig. 4. Impacts of the different parameters on the percentage of molten NEPCM (Fr_M): (a) Fr_M vs Re_f for various ω (b) Fr_M vs Re_f for various δ (c) Fr_M vs Re_f for various χ (d) Fr_M vs Re_f for various θ_f (e) Fr_M vs θ_f for various ω (f) Fr_M vs χ for various δ.

zones were shown - solidified, melted and liquified NEPCM core. NEPCM enters the domain with a solid core, which begins to melt while crossing the hot zone. As expected, the NEPCMs that are in close proximity to the tube wall, experience phase change sooner due to the temperature gradient in the layers of fluid near to tube wall. Similar to velocity and temperature boundary layers, a phase change boundary layer may be visualized in phase change phenomenon. The phase change boundary layer does not have a formal definition but can be understood in terms of heat penetration into the downstream of the mixture through conduction and convection after the mixture enters the domain. As the flow proceeds further, the absorbed heat is transferred to upstream layers, and as a result, the boundary layer develops until it reaches the fully developed region. It should be noted that the mixture undergoes phase change only when the fusion temperature of core is greater than tube wall temperature, and the mixture temperature is in the melting range temperature. This implies that in some conditions, while a thermal boundary layer is formed, the NEPCM suspension does not undergo phase change, and as a result, no phase change boundary layer emerges.

4. Description of solver and mesh sensitivity

The dimensionless governing equations were discretized using the Finite Volume Method (FVM), which, along with the applied boundary conditions were solved using SIMPLE algorithm to handle the pressur-

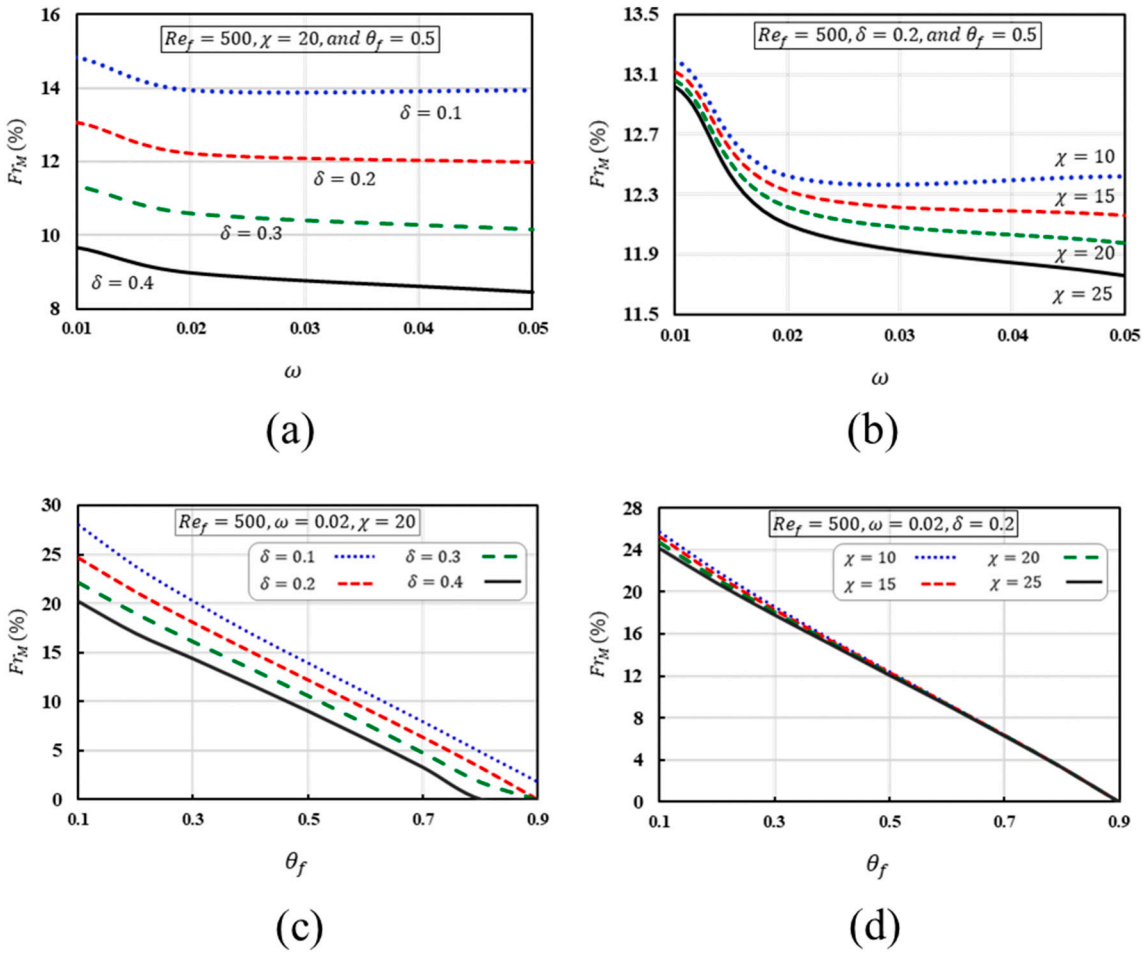

Fig. 5. Impacts of the different parameters on the percentage of molten NEPCM (Fr_M): (a) Fr_M vs ω for various δ (b) Fr_M vs ω for various χ (c) Fr_M vs θ_f for various δ (d) Fr_M vs θ_f for various χ.

e–velocity coupling. The properties of NEPCM and the mixture were updated by nanoFluid4Foam libraries at the beginning of each iteration. nanoFluid4Foam toolbox is an open-source toolbox, written in C++, to compute the thermophysical properties of mono or hybrid nanofluids with a wide range of different models [50]. In addition, it possesses the ability to perform two-phase modeling of nanofluids with different applicable boundary conditions for various applications from heat and mass transfer, and wastewater treatment to cardiovascular biomechanics and drug delivery [51,52]. To discretize the non-linear into linear algebraic equations, a Gauss upwind scheme and second-order corrected Gauss linear scheme were implemented for convective and conductive terms, respectively. The convergence criteria for pressure, velocity and temperature residuals were chosen to be 10^{-5}, 10^{-4} and 10^{-7}, respectively. A uniform structured mesh was generated in the R and Z directions. All calculations were carried out in OpenFOAM package using the nanoFluid4Foam toolbox.

To establish mesh independence, the average Nusselt number, based on Eq. (22) was calculated for several combinations of the total number of nodes in the *R* and *Z* directions. Problem parameters are $Re_f = 1000$, $\omega = 0.05, \delta = 0.3, \chi = 30, \theta_f = 0.5$. Table 7 summarizes the average Nusselt numbers obtained for different cases, showing that there was reasonable grid independence with around 50 and 300 nodes in the *R* and *Z* directions with a 0.03 % relative difference from the reference. Therefore, all subsequent calculations in this work were carried out with this level of discretization to have a precise result and lower run time.

5. Validation

Results from the present work were compared with several experimental investigations. In their investigation, Wang et al. [53]. measured Nu_{Loc} values along the tube length for forced convection heat transfer for a slurry comprised of 1-Bromohexadecane ($C_{16}H_{33}Br$) encapsulated PCM-water flow in a circular steel pipe with 4 mm diameter and 1.46 m length. Their study was carried out under the condition of *Re* ranging from 400 to 3500, wall heat fluxes ranging from 175.9 $W{\cdot}m^{-2}$ to 1063.6 $W{\cdot}m^{-2}$, and volume fractions from 0.05 to 0.2. For validation, the conditions were duplicated with an average uniform wall heat flux boundary condition of 296.8 $W{\cdot}m^{-2}$ and with 1-Bromohexadecane encapsulated particles with volume fraction of 5%. The fluid and MEPCM properties were set as: $Re = 441–538$, $k_{nf} = 0.568$, $C_{P,nf} = 4061$, $\rho_{nf} = 1001$, $\mu_{nf} = 1.57$ (mPa·s), $h_{sf} = 7\ kJ{\cdot}kg^{-1}$, and a melting temperature of 14 °C. Fig. 3(a) displays the evolution of the Nu_{Loc} along the tube length and compares results from the present study with the measurements reported by Wang et al. [53]. Our numerical results show good agreement with the cited experimental results, with only relatively small error (average 7.5 % error) between the two.

Moreover, a comparison between numerical results from the present work and an experimental study on convective heat transfer in a circular tube by Qiu et al. [54] is presented in Fig. 3(b), in which the local Nusselt number distribution along the tube length, from the present work and Qiu et al. [54] is plotted. They investigated forced convection heat transfer for a suspension consisting of water and MEPCM made of Melamine-Formaldehyde as wall material and solid paraffin as core

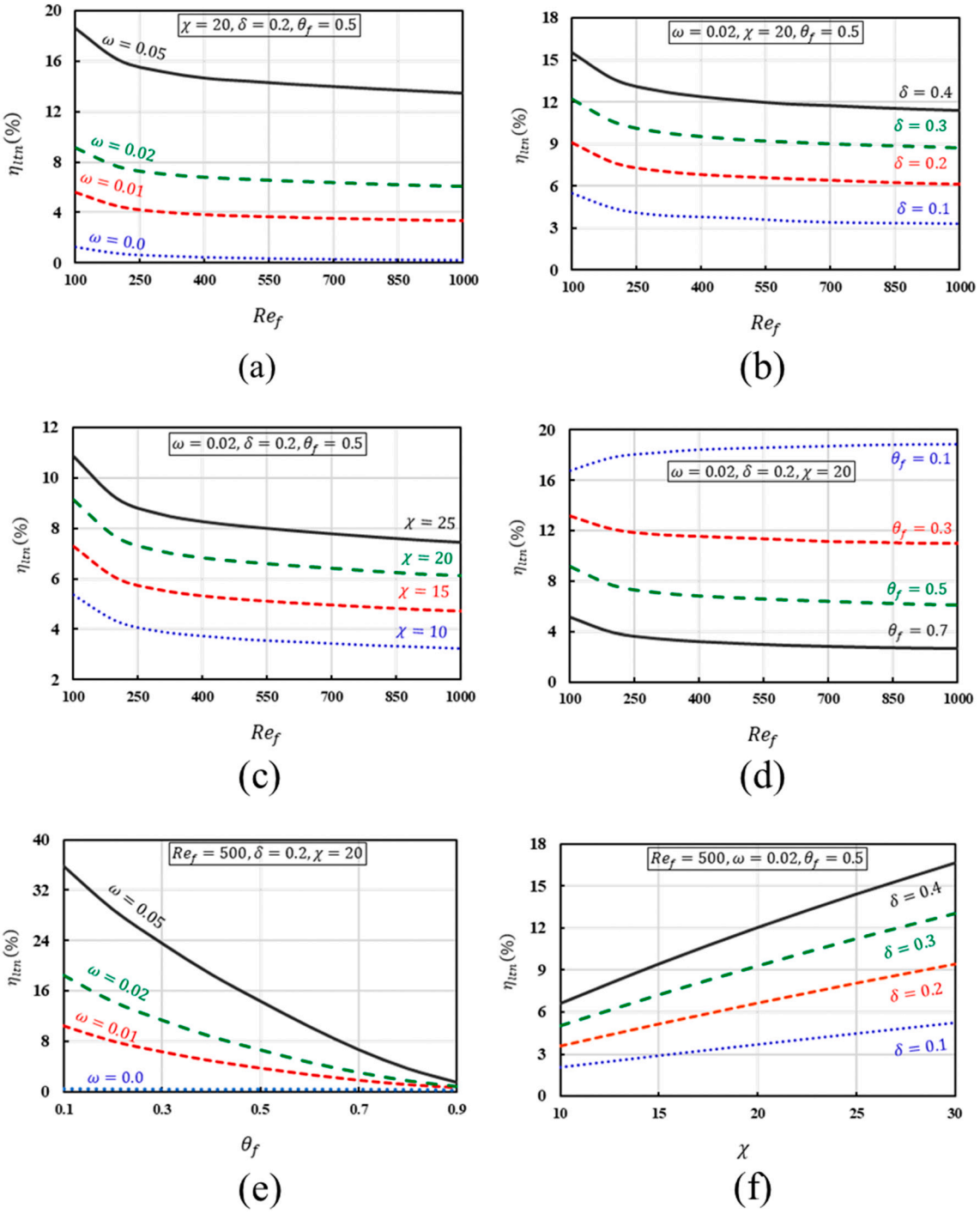

Fig. 6. Impacts of the different parameters on the latent heat efficiency (η_{ltn}): (a) η_{ltn} vs Re_f for various ω (b) η_{ltn} vs Re_f for various δ (c) η_{ltn} vs Re_f for various χ (d) η_{ltn} vs Re_f for various θ_f (e) η_{ltn} vs θ_f for various ω (f) η_{ltn} vs χ for various δ.

material. Experiments were carried out with flow speed of 0.510 m/s, $Re = 679$, heating rate of 225 W, and mass fraction of 5 %. As seen in Fig. 3(b), results from the present model are in good agreement with experimental measurements, with an average error of 6.3 %.

Another comparison was conducted with the experimental study of Zhang et al. [55] to assess the local Nusselt number versus the axial length. Zhang et al. [55] experimentally investigated the flow and heat transfer characteristics of water-MEPCMs laminar flow in a horizontal tube subject to a constant wall heat flux. The microcapsules comprised of paraffin core and highly crosslinked poly (methyl methacrylate) shell. The heat transfer test section was a 2.4 m circular tube with an internal diameter of 10 mm and 2 mm wall thickness. Other experimental conditions were $Re = 1148–1990$ for slurry, $u = 0.57$ m/s, $Q = 3500$ W, and mass fraction of 10 %. The simulations were performed for the present model based on the same conditions and the same thermophysical properties given in Zhang et al. [55]. Fig. 3(c) shows a comparison between the two, demonstrating very good agreement, with an average relative difference of 7 %.

Further, a comparison between numerical results from the present work and an experimental study on internal convective heat transfer in a circular tube by Chen et al. [56] is presented in Fig. 3(d), in which the local Nusselt number distribution along the tube length, both from the

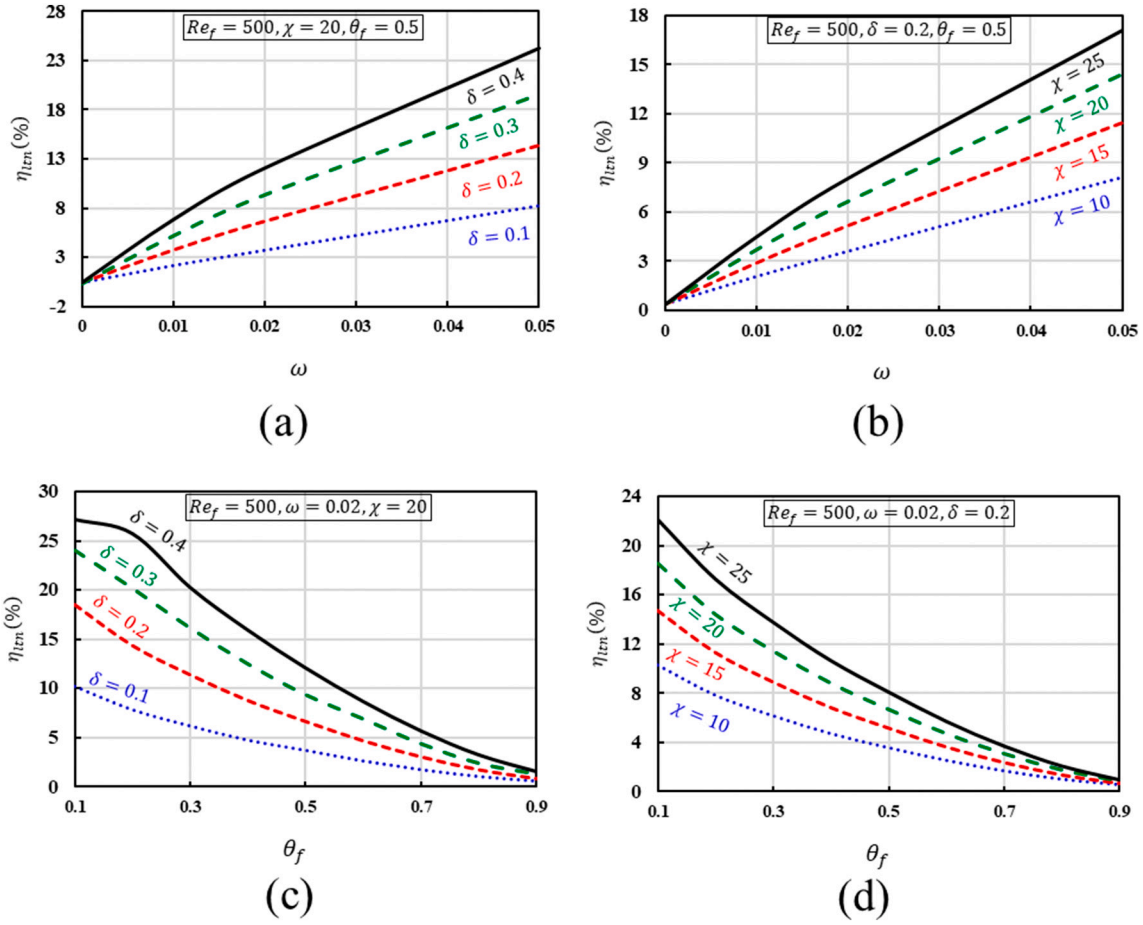

Fig. 7. Influence of the different parameters on the latent heat efficiency (η_{ltn}): (a) η_{ltn} vs ω for various δ (b) η_{ltn} vs ω for various χ (c) η_{ltn} vs θ_f for various δ (d) η_{ltn} vs θ_f for various χ.

present work and Chen et al. [56] is plotted at different values of *Re* and *Ste*. Chen et al. [56] investigated forced convection heat transfer for a suspension consisting of water and MEPCM with $d_P = 8.2\ \mu$m and an average mass fraction of 15.8 % inside a tube with uniform heat flux from the wall. Moreover, the following parameter values are applicable, based on the description of the experiment: $D = 4$ mm, $l = 1.46$ m, $416 \leq Re \leq 1438$, $1 \leq St \leq 2.8$, $Pr = 23.79$ and $h_{sf} = 20.5\ \left(\frac{\text{kJ}}{\text{kg}}\right)$. Even though there is a small shift between the experimental data and the present model, both show the same trend, and the worst-case deviation between the two is <10 %. Key sources of error that may be responsible for the relative shift between the two include modeling approximations and discretization errors on the computational side, and random errors due to variations in experimental conditions and measurement uncertainty related to measurement instruments in the experiments.

Finally, Zeinali et al. [57] have presented experimental measurements of forced convection of water-Al_2O_3 nanofluid inside a 3 mm diameter 1 m long tube. For the conditions used in this work, Table 8 presents a comparison between the present numerical calculations and previously reported experimental measurements for a volume fraction of 2 % aluminum nanoparticles. The two were in very close agreement, with a worst-case error of only 5.45 %. The good agreement obtained for this forced convection case provides further confidence in the present numerical set up.

6. Results and discussion

The main goal of the present work is to investigate the heat transfer rate and exergy losses due to the injection of NEPCM to the base fluid inside a tube, with uniform wall temperature. Dimensionless parameters studied in this work are broadly divided into two categories:

- Flow characteristics, including Reynolds number $(100 \leq Re_f \leq 1000)$.
- NEPCM characteristics encompassing the melting strength (MS) $(10 \leq \chi \leq 30)$, thickness of phase change zone (TPCZ) $(0.1 \leq \delta \leq 0.4)$, location of phase change zone (LPCZ) $(0.1 \leq \theta_f \leq 0.9)$, and mass fraction $(0 \leq \omega \leq 0.05)$.

A number of cases are simulated to study the effects of these parameters on the percentage of molten NEPCM particles at the tube outlet (Fr_M), variation of average Nusselt number (Nu_{Var}), latent heat efficiency (η_{ltn}), and variation of exergy losses ($X_{Var,Tot}$). These parameters are defined in subsequent sub-sections. The values of various parameters including $Pr_f, \lambda, L,$ and T_{amb} are 4.66, 0.438, 16.66, and 300 K, respectively, based on properties of water and NEPCM comprising n-eicosane and SLS.

6.1. Percentage of molten NEPCM particles at the tube outlet (Fr_M)

Figs. 4 and 5 plot the fraction of entering NEPCM particles that are melted at the tube outlet (Fr_M). Various cases shown in these plots show that an increase in Re_f and θ_f leads to a reduction in Fr_M. That is because an increase in Re_f corresponds to greater velocity of the mixture, due to which, there is insufficient time for phase change of the NEPCM. Additionally, as shown in Fig. 4(d), as θ_f increases, the phase change zone approaches the tube wall. As result, only a small part of the mixture is

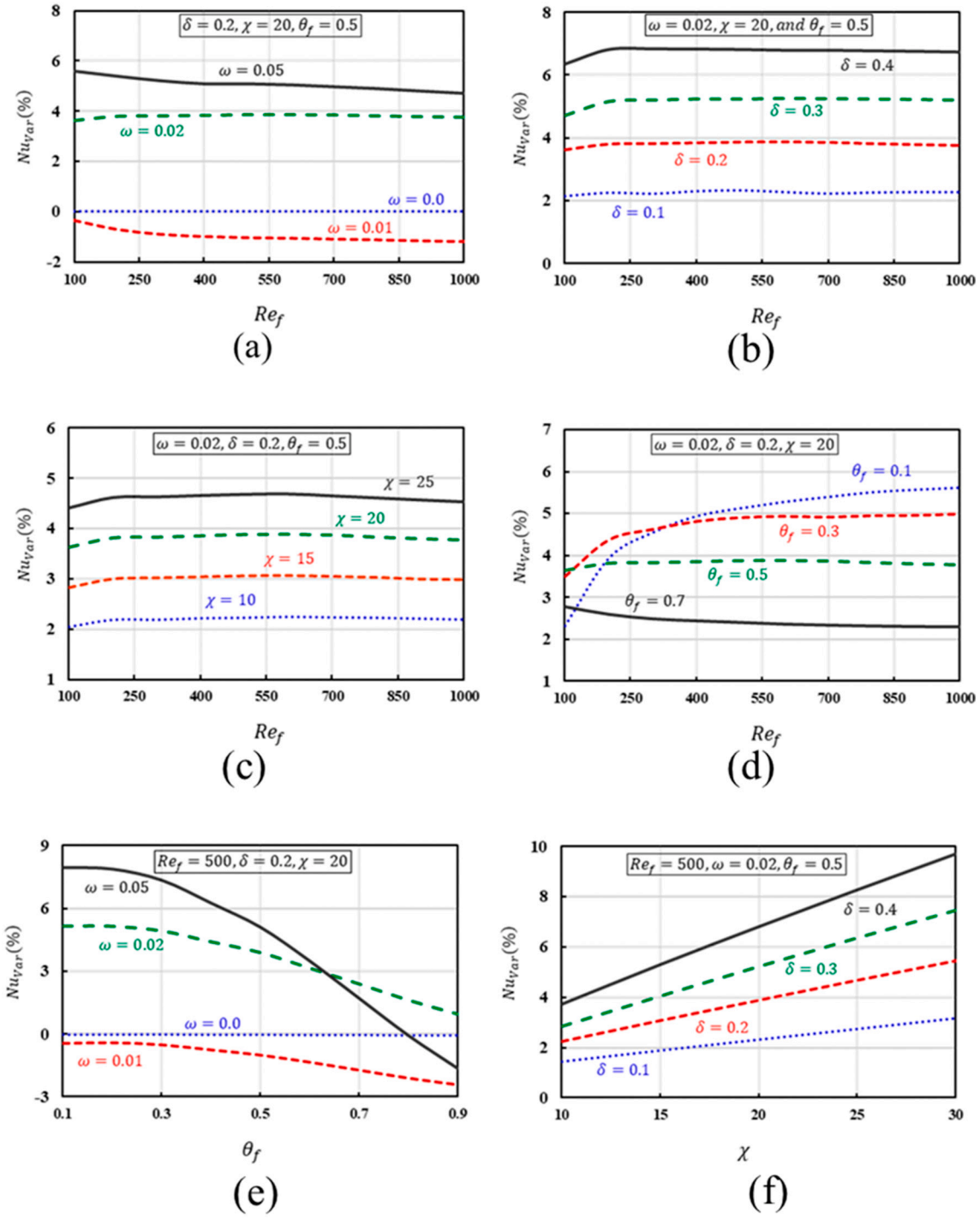

Fig. 8. Impacts of the different parameters on the variation of Nusselt number (Nu_{Var}): (a) Nu_{Var} vs Re_f for various ω (b) Nu_{Var} vs Re_f for various δ (c) Nu_{Var} vs Re_f for various χ (d) Nu_{Var} vs Re_f for various θ_f (e) Nu_{Var} vs θ_f for various ω (f) Nu_{Var} vs χ for various δ.

located at the phase change zone, and only a limited amount of NEPCM is melted. Moreover, according to Figs. 4(b), (f), 5(a), and (c), increasing δ contributes to reduction in Fr_M, because the phase transition zone is growing in thickness while the region where NEPCM are entirely melted is contracting (see Fig. 2(a)). It should be noted that the impact of ω and χ on Fr_M is relatively weaker, given that these parameters affect amplitude or strength of phase change zone (see Fig. 2(a)). As can be seen in Figs. 4(c), (f), and 5(d), Fr_M experiences only minor change as χ varies.

6.2. Impact of various parameters on latent heat efficiency (η_{ltn})

The latent heat efficiency η_{ltn}, defined as the ratio of latent heat to total received heat is calculated as follows:

$$\eta_{ltn}(\%) = \frac{\dot{Q}_{latent}}{\dot{Q}_{tot}} \times 100 \tag{25}$$

where $\dot{Q}_{latent}$, and $\dot{Q}_{tot}$ are the heat received as latent heat and total heat, respectively. Further, one may write:

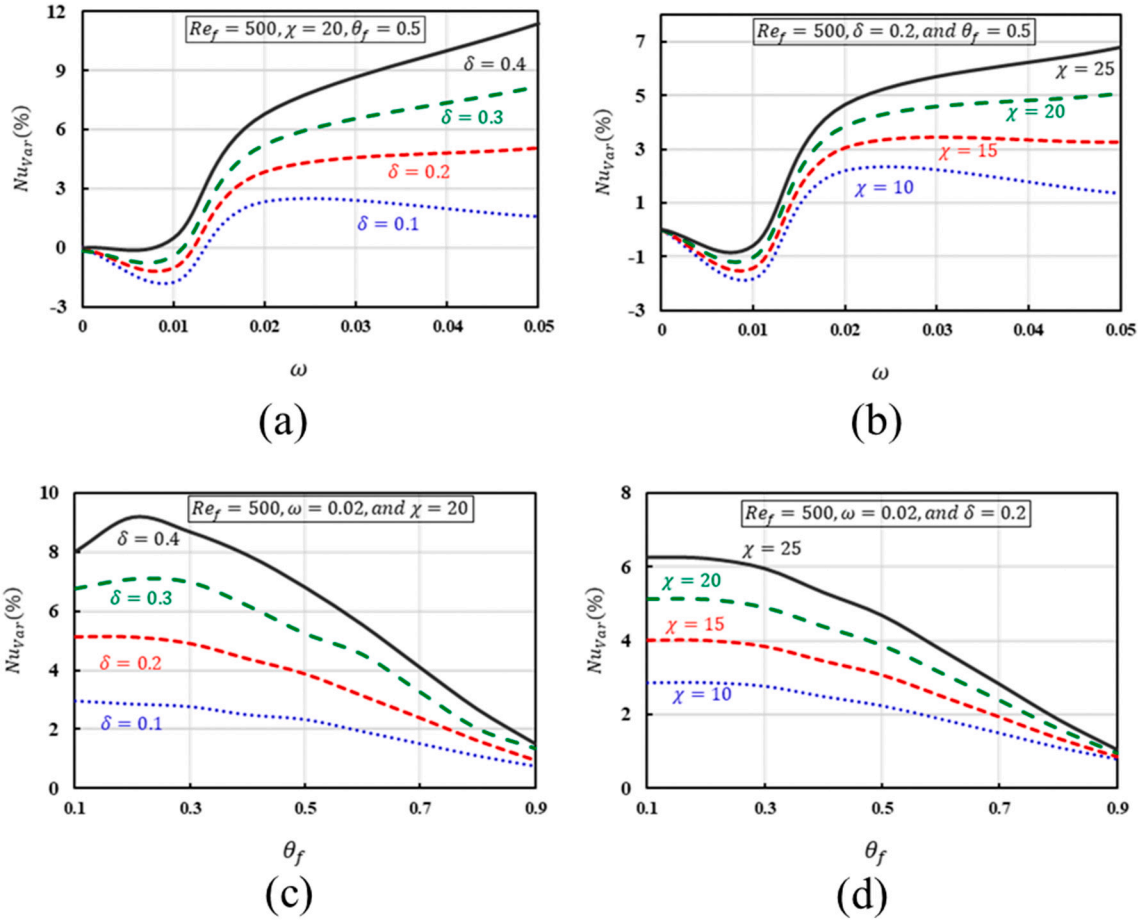

Fig. 9. Influence of the different parameters on the variation of Nusselt number (Nu_{Var}): (a) Nu_{Var} vs ω for various δ (b) Nu_{Var} vs ω for various χ (c) Nu_{Var} vs θ_f for various δ (d) Nu_{Var} vs θ_f for various χ.

$$\dot{Q}_{latent} = k_m \left(\frac{\partial T}{\partial r}\right)_{r=D/2} - \dot{m} C_{P,m0} (T_{out} - T_{in}) \tag{26}$$

where $\dot{m} = \rho_m V_{In} \frac{\pi D^2}{4}$ is the mass flow rate.

The latent heat efficiency as defined above facilitates a better understanding of the NEPCM melting process. η_{ltn} can be related to various input parameters on the basis of the theory discussed above. These relationships are depicted in detail in Figs. 6 and 7. As evident from Fig. 6 (a), (b), (c), and (d), increasing Re_f is found to decrease η_{ltn} for all ω, δ, and χ because of reduced time available for NEPCM to melt. Based on Fig. 6(d), increasing Re_f is found to enhance η_{ltn} for $\theta_f = 0.1$ and decrease η_{ltn} for $\theta_f > 0.1$, since the location of energy wall approaches the hot wall. Further, increasing ω, δ and χ enhances η_{ltn}, strength of energy wall (SEW), and thickness of energy wall (TEW) to receive more heat. Finally, increasing θ_f results in lower η_{ltn} because Fr_M is reduced.

6.3. Effect of different parameters on variation of average Nusselt number (Nu_{Var})

The Nusselt number can be interpreted as the dimensionless temperature gradient on the wall or the ratio of convective to conductive heat transfer. Furthermore, the dimensionless energy equation given by Eq. (15) shows that Nusselt number depends on Reynolds and Prandtl numbers of the base fluid, as well as *Cr*, which is a function of dimensionless parameters including volume fraction φ, strength χ, thickness δ, and location of energy wall (θ_f).

$$Nu = \frac{d\theta}{dr} \text{ at } r = 1 = f(Cr, Pr_f, Re_f) Nu = \frac{d\theta}{dr} \text{ at } r = 1 = f(Cr, Pr_f, Re_f) \tag{27}$$

Moreover, the dimensionless bulk temperature, local and average Nusselt number of the tube can be obtained as follows:

$$\theta_b(Z) = 8 \int_0^{1/2} \theta(R, Z) V_Z(R)\, R dR \tag{28}$$

$$Nu_{loc}(Z) = \frac{1}{\theta_b(Z)} \left(\frac{\partial \theta}{\partial R}\right)_{R=1/2} \tag{29}$$

$$Nu_{ave} = \frac{1}{L} \int_0^L Nu_{loc}(Z)\, dZ \tag{30}$$

Subscripts $f, m, b, loc,$ and *ave* represent the base fluid, mixture of water/NEPCM, bulk, local, and average, respectively. In the present work, the variation of Nusselt number is defined as follows:

$$Nu_{Var}(\%) = \frac{Nu_{NEPCM} - Nu_{baseline}}{Nu_{baseline}} \times 100 \tag{31}$$

where $Nu_{baseline}$ and Nu_{NEPCM} refer to the computed Nusselt number for the baseline case (no NEPCM) and for the case with NEPCM present in the base fluid, where both are calculated at the same Reynolds number. In this manner, Nu_{Var} captures the effect of adding NEPCM to the pure base fluid.

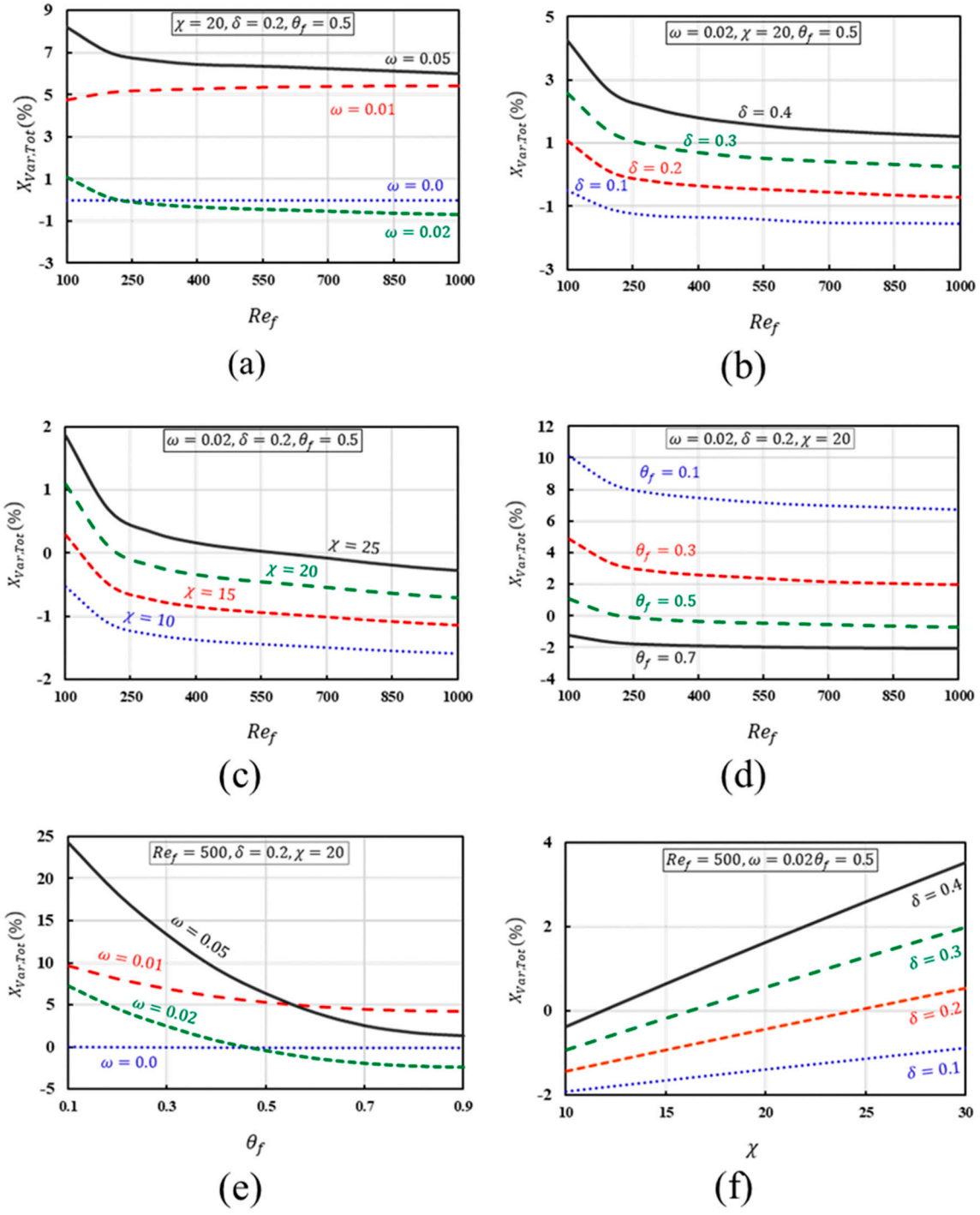

Fig. 10. Influence of the different parameters on the variation of total exergy losses ($X_{Var,Tot}$): (a) $X_{Var,Tot}$ vs Re_f for various ω (b) $X_{Var,Tot}$ vs Re_f for various δ (c) $X_{Var,Tot}$ vs Re_f for various χ (d) $X_{Var,Tot}$ vs Re_f for various θ_f (e) $X_{Var,Tot}$ vs θ_f for various ω (f) $X_{Var,Tot}$ vs χ for various δ.

In this manner, the Nu_{Var} captures the effect of adding NEPCM to the pure base fluid. Figs. 8 and 9 demonstrate the impact of various problem parameters in Nu_{var}.

Figs. 8 and 9 demonstrate the impact of various problem parameters in Nu_{var}. Fig. 8 (a), (b), (c), and (d) show that in each case, Nu_{Var} remains largely independent of Re_f. Increasing Re_f is found to result in a drop-off in Fr_M, although it does increase the temperature gradient. Accordingly, these effects act against each other. Although enhancing Re_f reduces Fr_M and does not influence η_{ltn}, however, it augments Nu_{Var} for $\theta_f = 0.1$ and 0.3, with the convective heat transfer enhanced as a result of Fr_M enhancement (see Fig. 8 (d)). In addition, Nu_{Var} is independent of Re_f for $\theta_f > 0.3$. According to Fig. 8 (e) for variation of Nu_{Ave} at $Re_f = 500$, adding $\omega = 0.01$ of NEPCM to water reduces Nu_{Ave}. Also, this reduction in Nu_{Ave} is clearly observable when $\omega = 0.05$ for $\theta_f > 0.8$. Moreover, Nu_{Ave} is found to increase by up to 5 % and 8 % by adding $\omega = 0.02$ and $\omega = 0.05$ NEPCM to water due to enhancement of SEW, respectively. It is to be noted that that the enhancement of θ_f decreases Nu_{Ave} due to a reduction in Fr_M and η_{ltn} (reduction in convective heat transfer). In Fig. 9 (a) and (b), adding $\omega = 0.01$ of NEPCM to water reduces Nu_{Ave}, and adding $\omega = 0.02$ and 0.05 elevates Nu_{Ave} relative to pure water due to the impact of thermal conductivity. As is clear from all cases shown in Figs. 8 and 9, increasing δ and χ enhances Nu_{Ave} by augmenting SEW.

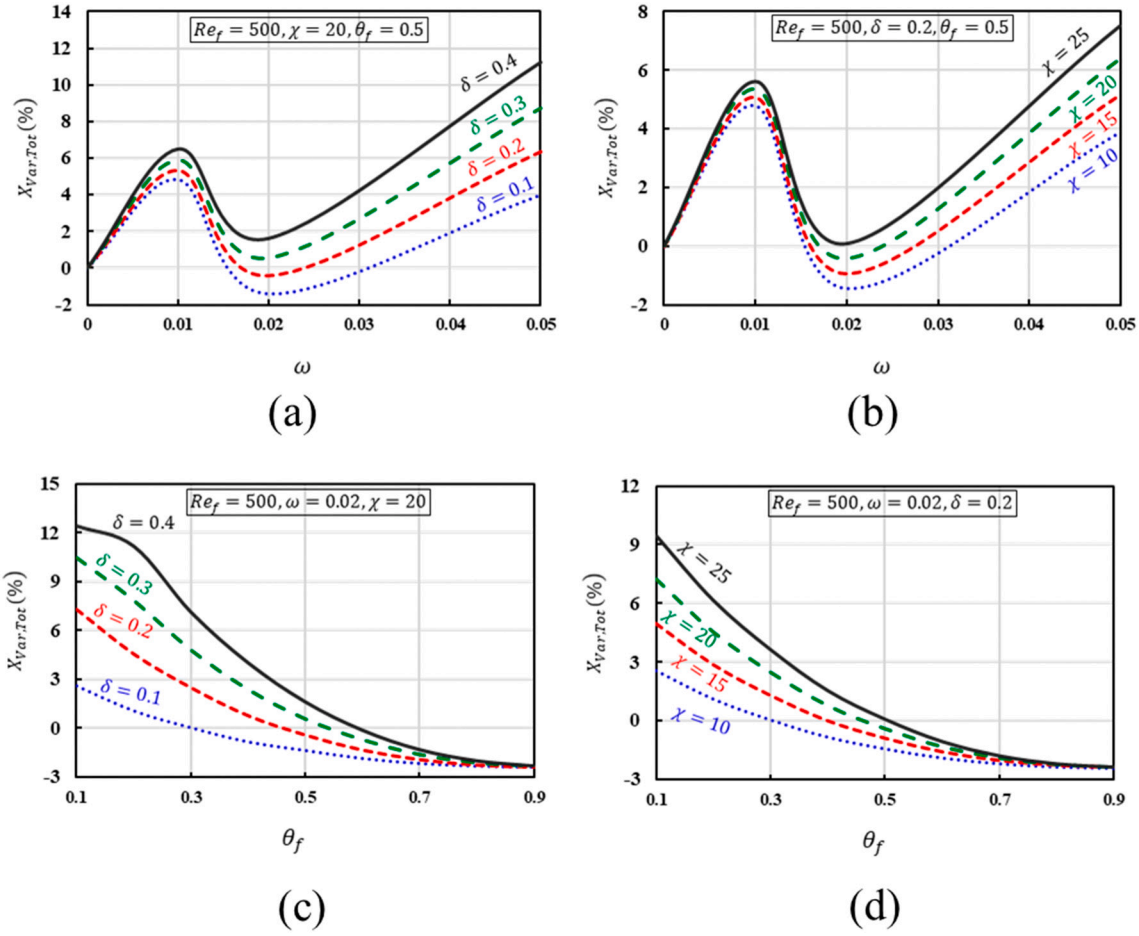

Fig. 11. Influence of the different parameters on the variation of total exergy losses ($X_{Var,Tot}$): (a) $X_{Var,Tot}$ vs ω for various δ (b) $X_{Var,Tot}$ vs ω for various χ (c) $X_{Var,Tot}$ vs θ_f for various δ (d) $X_{Var,Tot}$ vs θ_f for various χ.

6.4. *Impact of various parameters on dimensionless exergy losses ($X_{Var,T}$)*

Heat transfer and fluid friction owing to temperature and velocity gradient are two dominant entropy generation mechanisms in forced convection heat transfer problems. By multiplying T_{Amb} to the entropy generation, dimensionless form of exergy losses can be achieved as follows:

$$X_{Loc,FF} = \frac{Br}{\Omega}\left(\frac{\mu_m}{\mu_f}\right)\left[2\left(\left(\frac{\partial V_R}{\partial R}\right)^2 + \left(\frac{V_R}{R}\right)^2 + \left(\frac{\partial V_Z}{\partial Z}\right)^2\right) + \left(\frac{\partial V_Z}{\partial R} + \frac{\partial V_R}{\partial Z}\right)^2\right] \tag{32}$$

$$X_{Loc,HT} = \left(\frac{k_m}{k_f}\right)\left[\left(\frac{\partial \theta}{\partial R}\right)^2 + \left(\frac{\partial \theta}{\partial Z}\right)^2\right] \tag{33}$$

$$X_{Tot} = \int \left(X_{Loc,FF} + X_{Loc,HT}\right) dV \tag{34}$$

$$\mathrm{Br} = \frac{\mathrm{V_{In}}^2 \mu_f}{k_f \Delta T} \tag{35}$$

$$\Omega = \frac{\Delta T}{T_f} \tag{36}$$

where X_{FF} and X_{HT} are the fluid friction and heat transfer related exergy losses. The Brinkman number (Br) is a nondimensional number representing the ratio of heat generated due to friction between different layers of a viscous fluid and heat conduction in that fluid. For the parameters used in this work, it is found that $7.638 \times 10^{-8} < Br < 3.055 \times 10^{-5}$, and $0.066 < \Omega < 0.0166$. As a result, the effects of exergy losses due to fluid friction can be shown to be negligible compared to contributions from temperature gradient. Further, the variation of exergy losses can be calculated as below:

$$X_{Var,Tot}(\%) = \frac{X_{NEPCM} - X_{baseline}}{X_{baseline}} \times 100 \tag{37}$$

Figs. 10 and 11 present the effect of adding NEPCM to base fluid on exergy losses. It is to be noted that the phase change material does not produce entropy. In fact, the NEPCM may alleviate exergy losses by receiving heat as latent heat. Fig. 10 (a), (b), (c), and (d) show that increasing Re_f results in reduction in exergy losses relative to the base fluid. This is explained based on the amelioration of the temperature gradient due to addition of NEPCM, which contributes to reduction in exergy losses. Figs. 10(e), 11(c) and (d) also show that for all values of ω, δ and χ considered, exergy losses are inversely related to θ_f. Further, increasing χ and δ increases exergy losses because of the temperature gradient enhancement. In general, exergy loss is a function of how thermal conductivity varies with ω. It can be concluded from Fig. 11 (a) and (b) that adding 1 % of NEPCM to the base fluid increases the thermal conductivity and exergy losses up to 5 %. However, utilizing $\omega = 0.02$ of NEPCM reduces thermal conductivity and exergy losses. Eventually, it is found that adding $\omega > 0.02$ can intensify exergy losses. Therefore, the optimum value of ω for minimizing exergy losses is around $\omega = 0.02$. This is in contrast with past work that advocates large mass fractions by

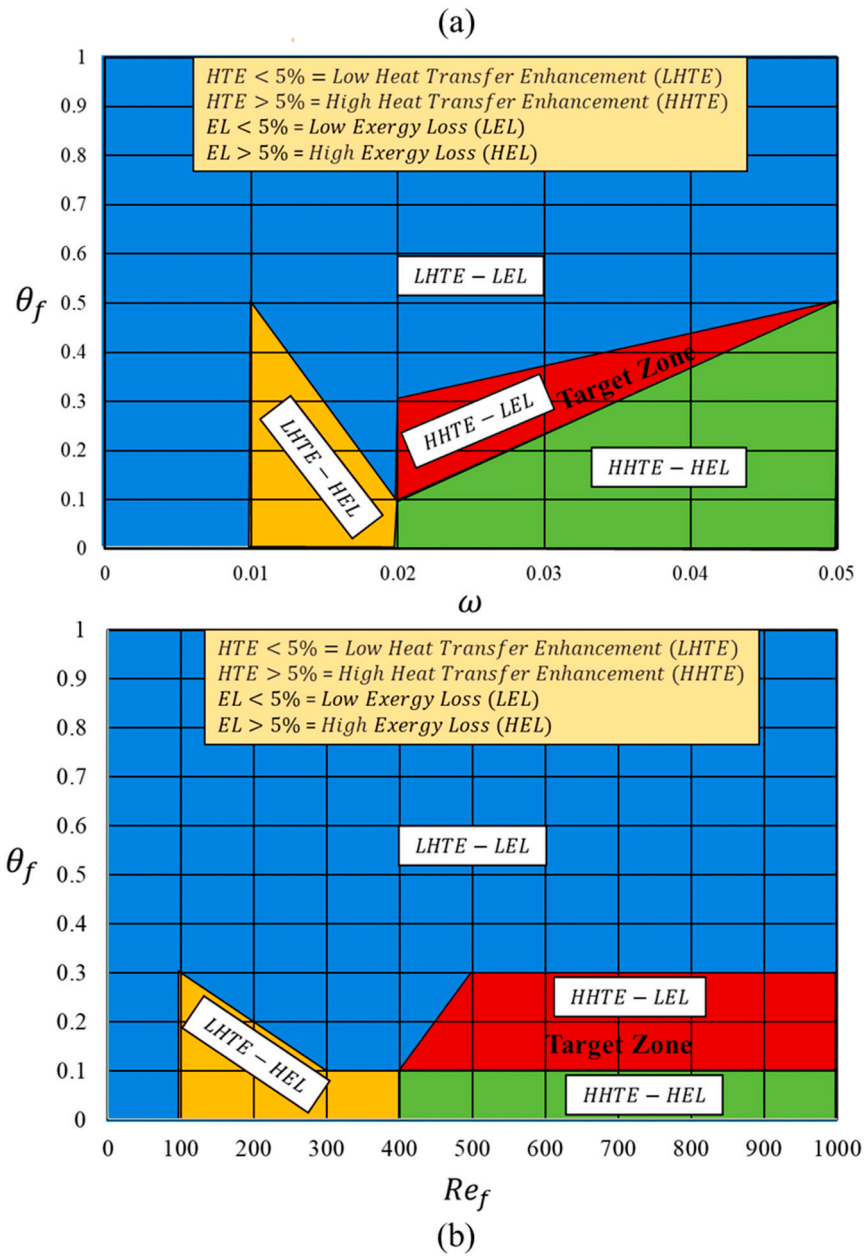

Fig. 12. The impacts of melting parameter (θ_f) and physical parameters (*Re* and ω) on heat transfer enhancement-exergy losses regime map for: (a) $\chi = 20, \delta = 0.2,$ and $Re_f = 500$. (b) $\chi = 20, \delta = 0.2,$ and $\omega = 0.02$.

ignoring the impact on exergy losses. Note that the model presented here is general enough to evaluate this optimal value of other set of parameters as well.

Analysis of natural convection of water-NEPCM [31] has demonstrated the importance of the volume of NEPCM in the phase change zone, and not the melted volume, since it enhances both specific heat capacity and Prandtl number. In contrast, results for forced convection in this work elucidate that the volume of the melted NEPCM at the tube outlet is important, and not the volume of NEPCM in the phase change zone. This is because the more melted the NEPCMs are at the exit of the tube, the more heat they receive as latent heat, which reduces the temperature of the domain and increases the heat transfer rate. In the context of the present study, the average convective heat transfer coefficient (h_{Var}) can be calculated as follows:

$$h_{Var} = \frac{k_m}{k_f}(1 + Nu_{Var}) - 1 \tag{38}$$

Therefore, h_{Var} can, in principle, be negative if $Nu_{Var} > \frac{k_f}{k_m} - 1$.

In the present work, average Nusselt number, heat transfer rate, exergy losses are enhanced by 9.3 %, 16.1 % and 17 %, respectively, relative to pure water for NEPCMs for $Re_f = 1000, \omega = 0.05, \chi = 20, \delta = 0.2$ and $\theta_f = 0.1$. In comparison, for $Re_f = 500, \omega = 0.02, \chi = 20, \delta = 0.4$ and $\theta_f = 0.5$, the Nusselt number and heat transfer rate improve by 6.2 % and 2.5 %, respectively, while the exergy losses are zero since the phase change materials do not produce entropy. These calculations demonstrate the importance of the present simulations in understanding the exergy characteristics of this forced convection flow problem.

A figure is provided that summarizes all of the results into an operating regime map. Fig. 12 shows regions of heat transfer enhancement and exergy loss as a function of the most important non-dimensional parameters for melting (θ_f), flow (*Re*) and loading mass fraction (ω). As it is evident from Fig. 12(a) and (b), only a limited zone can be considered as the most favorable condition to enhance the heat transfer

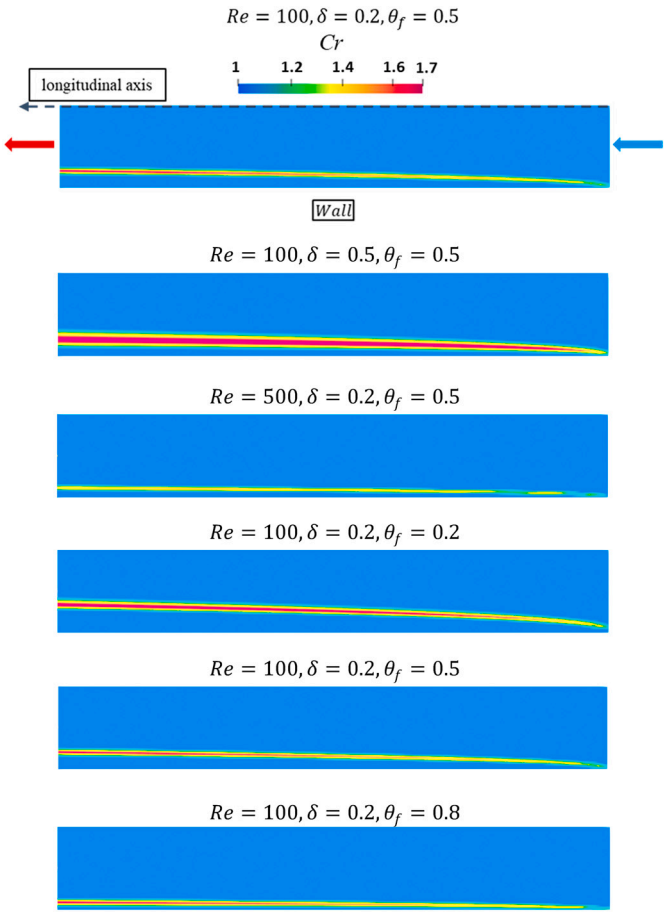

Fig. 13. Cr contours for $\omega = 0.02$ and $\chi = 20$ for different Reynolds numbers (100 and 500), δ (0.2 and 0.5), and θ_f (0.2, 0.5, and 0.8).

enhancement while keep the exergy losses in check, namely $0.1 \leq \theta_f \leq 0.3$, $400 < Re \leq 1000$, and $2\ \% \leq \omega < 5\ \%$ (see *HHTE-LEL* regions).

Fig. 13 plots *Cr* contours for a section at $z = 0$ *to* $L/5$ for $\omega = 0.02$ and $\chi = 20$ when the NEPCM-water flow enters the tube from the right side. The phase change boundary layer referring to NEPCM in the melting zone is plotted for a number of different flow conditions. It is only when the mixture temperature is within the melting range that the mixture undergoes phase change. It can be inferred from Fig. 13 that increasing δ makes the melting zone thicker due to reduced temperature difference between the tube wall and inlet. Additionally, because the thermal boundary layer becomes thinner as *Re* increases, the phase change boundary layer approaches the tube wall. Moreover, as shown in Fig. 13, the melting zone approaches the tube wall when θ_f increases since increasing θ_f implies that NEPCMs have to be melted at higher temperatures (note that maximum temperature of the system is at the wall).

7. Conclusions

Almost every thermal energy system utilizes fluid flow inside tubes and, as such, can benefit from enhanced heat convective transfer. In this regard, NEPCMs represent a promising method for heat transfer enhancement, but if such systems are designed solely based upon their heat transfer rate (as has been done in all prior NEPCM/MEPCM literature), exergy destruction due to the inclusion of NEPCM/MEPCM will be overlooked. Additionally, the model developed here can investigate the impact of a number of non-dimensional parameters including and beyond the commonly studied ones such as flow rate and NEPCM concentration. Considering these crucial parameters shifts the design of NEPCM-based thermal systems from low to highly efficient and cost-effective systems. The key contribution of the present work is a detailed analysis of laminar flow in tube with NEPCM-water to determine how the addition of the NEPCMs can be used to boost the heat transfer rate while reducing exergy losses. The important dimensionless parameters for this problem are found to be melting strength (χ), thickness (δ) and location (θ_f) of phase change zone (TPCZ and LPCZ), Reynolds number (Re_f) and the mass fraction of NEPCM (ω). A comprehensive investigation of the impact of these parameters on the percentage of the molten NEPCM particles at the outlet, average Nusselt number, latent heat efficiency, and the exergy losses was presented.

First of all, it was shown that when the location of phase change (θ_f) increases from 0.1 to 0.9, only a small portion of NEPCM melts, and therefore, the percentage of molten NEPCM (Fr_M) would undergo a significant decrement (around 48 %). Moreover, increasing the thickness of the phase change (δ) from 0.1 to 0.4 causes a 42 % drop-off in the percentage of molten NEPCM (Fr_M) as the thickness of the phase change zone grows, contributing to placing more NEPCM in the phase change zone rather than causing complete melting. More importantly, the percentage of molten NEPCM (Fr_M) is found to reduce when Re_f and θ_f increase. Therefore, the latent heat efficiency (η_{ltn}) diminishes except when the location of phase change is near to the minimum temperature of the system (i.e., near the temperature of the mixture at inlet). It is worth mentioning that the region of phase change in the tube is limited and the improvement of heat transfer is hampered when the location of phase change (θ_f) approaches to the maximum temperature of the system, (i.e., the tube wall). Lastly, altering the melting strength (χ) and thickness of phase change zone (δ) have only limited impact on the percentage of molten NEPCM and latent heat thermal efficiency, compared to the impact of other parameters.

Overall, the current work has revealed that it is feasible to have a lower mass fraction while benefiting from enhanced heat transfer without adding significant exergy losses. The best design conditions found in this analysis have a much lower mass fraction (i.e., $2\ \% \leq \omega < 5\ \%$) than most recent studies (which propose $5\ \% < \omega < 30\ \%$). Moreover, it is recommended to choose $0.1 \leq \theta_f \leq 0.3$ and $0.2 \leq \delta \leq 0.3$. The authors propose that future studies should consider a combination of parameters including melting strength (χ), thickness (δ) and location (θ_f) of phase change to ensure the heat transfer enhancement, while the exergy losses do not exceed in NEPCM-based thermal systems.

CRediT authorship contribution statement

All authors contributed in writing and analysis for this manuscript.

Declaration of competing interest

The authors declared that there is no conflict of interest.

Data availability

Data will be made available on request.

References

[1] M. Torabi, N. Karimi, G.P. Peterson, S. Yee, Challenges and progress on the modelling of entropy generation in porous media: a review, Int. J. Heat Mass Transf. 114 (2017) 31–46.
[2] A. Sciacovelli, V. Verda, E. Sciubba, Entropy generation analysis as a design tool—a review, Renew. Sust. Energ. Rev. 43 (2015) 1167–1181.
[3] M. Bahiraei, N. Mazaheri, H. Moayedi, Entropy generation and exergy destruction for flow of a biologically functionalized graphene nanoplatelets nanofluid within tube enhanced with a novel rotary coaxial cross double-twisted tape, Int. Commun. Heat Mass Transfer 113 (2020), 104546.
[4] R.R.J. Al Doury, T.K. Salem, I.T. Nazzal, R. Kumar, M. Sadeghzadeh, A novel developed method to study the energy/exergy flows of buildings compared to the traditional method, J. Therm. Anal. Calorim. (2020) 1–11.

[5] J.M. Avellaneda, F. Bataille, A. Toutant, G. Flamant, Variational entropy generation minimization of a channel flow: convective heat transfer in a gas flow, Int. J. Heat Mass Transf. 160 (2020), 120168.
[6] Y. Han, X.S. Wang, H.N. Zhang, Q.Z. Chen, Z. Zhang, Multi-objective optimization of helically coiled tube heat exchanger based on entropy generation theory, Int. J. Therm. Sci. 147 (2020), 106150.
[7] R. Sarma, A.K. Shukla, H.S. Gaikwad, P.K. Mondal, S. Wongwises, Effect of conjugate heat transfer on the thermo-electro-hydrodynamics of nanofluids: entropy optimization analysis, J. Therm. Anal. Calorim. (2020) 1–16.
[8] S. Rashidi, M. Akbarzadeh, R. Masoodi, E.M. Languri, Thermal-hydraulic and entropy generation analysis for turbulent flow inside a corrugated channel, Int. J. Heat Mass Transf. 109 (2017) 812–823.
[9] B. Vahedi, E. Golab, A.N. Sadr, K. Vafai, Thermal, thermodynamic and exergoeconomic investigation of a parabolic trough collector utilizing nanofluids, Appl. Therm. Eng. 206 (2022), 118117.
[10] K. Khanafer, K. Vafai, A critical synthesis of thermophysical characteristics of nanofluids, Int. J. Heat Mass Transf. 54 (19–20) (2011) 4410–4428.
[11] R.A. Taylor, P.E. Phelan, T.P. Otanicar, C.A. Walker, M. Nguyen, S. Trimble, R. Prasher, Applicability of nanofluids in high flux solar collectors, J. Renew. Sustain. Energy 3 (2) (2011), 023104.
[12] K. Vafai, H.C. Tien, A numerical investigation of phase change effects in porous materials, Int. J. Heat Mass Transf. 32 (1989) 1261–1277.
[13] M. Shekaramiz, S. Fathi, H.A. Ataabadi, H. Kazemi-Varnamkhasti, D. Toghraie, MHD nanofluid free convection inside the wavy triangular cavity considering periodic temperature boundary condition and velocity slip mechanisms, Int. J. Therm. Sci. 170 (2021), 107179.
[14] A. Albojamal, H. Hamzah, K. Vafai, Energy storage analysis of phase change materials (PCMs) integrated with thermal conductivity enhancers (TCEs), Numer. Heat Transfer Part A Appl. 83 (1) (2022) 1–18.
[15] N. Shirani, D. Toghraie, S. Rostami, Comparative study of mixed convection heat transfer of water–Cu nanofluid in an enclosure having multiple rotating circular cylinders with different configurations and considering harmonic cylinders rotation, J. Therm. Anal. Calorim. 144 (2021) 1557–1570.
[16] A. Albojamal, K. Vafai, Analysis of particle deposition of nanofluid flow through porous media, Int. J. Heat Mass Transf. 161 (2020), 120227.
[17] R. Sureshkumar, S.T. Mohideen, N. Nethaji, Heat transfer characteristics of nanofluids in heat pipes: a review, Renew. Sust. Energ. Rev. 20 (2013) 397–410.
[18] K. Khanafer, K. Vafai, Application of nanofluids in heat transfer enhancement of refrigeration systems, Nanofluids Eng. Appl. (2019) 143–160.
[19] S. Lee, R.A. Taylor, L. Dai, R. Prasher, P.E. Phelan, The effective latent heat of aqueous nanofluids, Materials Research Express 2 (6) (2015), 065004.
[20] M. Parhizi, A. Jain, The impact of thermal properties on performance of phase change based energy storage systems, Appl. Therm. Eng. 162 (2019), 114154.
[21] A. Papadimitratos, S. Sobhansarbandi, V. Pozdin, A. Zakhidov, F. Hassanipour, Evacuated tube solar collectors integrated with phase change materials, Sol. Energy 129 (2016) 10–19.
[22] V. Bianco, M. De Rosa, K. Vafai, Phase-change materials for thermal management of electronic devices, Appl. Therm. Eng. 214 (2022), 118839.
[23] A. Mostafavi, A. Jain, Thermal management effectiveness and efficiency of a fin surrounded by a phase change material (PCM), Int. J. Heat Mass Transf. 191 (2022), 122630.
[24] H. Kazemi-Varnamkhasti, I. Khazaee, M. Ameri, D. Toghraie, Heat storage and increasing the rate of heat transfer in polymer electrolyte membrane fuel cell by adding nano-encapsulated phase change material to water in the cooling process, J. Energy Storage 59 (2023), 106497.
[25] A. Mostafavi, M. Parhizi, A. Jain, Semi-analytical thermal modeling of transverse and longitudinal fins in a cylindrical phase change energy storage system, Int. J. Therm. Sci. 153 (2020), 106352.
[26] A. Ghahremannezhad, H. Xu, M.R. Salimpour, P. Wang, K. Vafai, Thermal performance analysis of phase change materials (PCMs) embedded in gradient porous metal foams, Appl. Therm. Eng. 179 (2020), 115731.
[27] K. Tumuluri, J.L. Alvarado, H. Taherian, C. Marsh, Thermal performance of a novel heat transfer fluid containing multiwalled carbon nanotubes and microencapsulated phase change materials, Int. J. Heat Mass Transf. 54 (25–26) (2011) 5554–5567.
[28] F. Hassanipour, J. Lage, Enhanced mini-channel forced convection with encapsulated phase-change particles, January, in: Heat Transfer Summer Conference 48487, 2008, pp. 745–754.
[29] G. Zhang, G. Cui, B. Dou, Z. Wang, M.A. Goula, An experimental investigation of forced convection heat transfer with novel microencapsulated phase change material slurries in a circular tube under constant heat flux, Energy Convers. Manag. 171 (2018) 699–709.
[30] H. Lu, H.R. Seyf, Y. Zhang, H.B. Ma, Heat transfer enhancement of backward-facing step flow by using nano-encapsulated phase change material slurry, Numer. Heat Transfer Part A Appl. 67 (4) (2015) 381–400.
[31] E. Golab, S. Goudarzi, H. Kazemi-Varnamkhasti, H. Amigh, F. Ghaemi, D. Baleanu, A. Karimipour, Investigation of the effect of adding nano-encapsulated phase change material to water in natural convection inside a rectangular cavity, J. Energy Storage 40 (2021), 102699.
[32] M. Moshtagh, A. Jamekhorshid, A. Azari, M.M. Farid, Experimental and numerical investigation of microencapsulated phase change material slurry heat transfer inside a tube with butterfly tube inserts, Appl. Therm. Eng. 174 (2020), 115270.
[33] R. Sabbah, J. Seyed-Yagoobi, S. Al-Hallaj, Heat transfer characteristics of liquid flow with micro-encapsulated phase change material: numerical study, J. Heat Transf. 133 (12) (2011).
[34] M. Kong, J.L. Alvarado, E.M. Languri, An experimental study of heat transfer characteristics of microencapsulated phase change material slurry in a coil heat exchanger, November, in: ASME International Mechanical Engineering Congress and Exposition 56352, American Society of Mechanical Engineers, 2013. V08BT09A041.
[35] J. Yang, D. Hutchins, C.Y. Zhao, Melting behaviour of differently-sized micro-particles in a pipe flow under constant heat flux, Int. Commun. Heat Mass Transfer 53 (2014) 64–70.
[36] M.S. Ghoghaei, A. Mahmoudian, O. Mohammadi, M.B. Shafii, H. Jafari Mosleh, M. Zandieh, M.H. Ahmadi, A review on the applications of micro-/nano-encapsulated phase change material slurry in heat transfer and thermal storage systems, J. Therm. Anal. Calorim. 145 (2) (2021) 245–268.
[37] Y.M. El Hasadi, J.M. Khodadadi, Numerical simulation of the effect of the size of suspensions on the solidification process of nanoparticle-enhanced phase change materials, J. Heat Transf. 135 (5) (2013).
[38] K.Y. Leong, M.R.A. Rahman, B.A. Gurunathan, Nano-enhanced phase change materials: a review of thermo-physical properties, applications and challenges, J. Energy Storage 21 (2019) 18–31.
[39] W.J. Minkowycz, E.M. Sparrow, J.P. Abraham (Eds.), Nanoparticle Heat Transfer and Fluid Flow 4, CRC PRESS, 2012.
[40] D. Lilley, J. Lau, C. Dames, S. Kaur, R. Prasher, Impact of size and thermal gradient on supercooling of phase change materials for thermal energy storage, Appl. Energy 290 (2021), 116635.
[41] N.S. Dhaidan, J.M. Khodadadi, T.A. Al-Hattab, S.M. Al-Mashat, Experimental and numerical investigation of melting of phase change material/nanoparticle suspensions in a square container subjected to a constant heat flux, Int. J. Heat Mass Transf. 66 (2013) 672–683.
[42] Z. Rao, S. Wang, F. Peng, Molecular dynamics simulations of nano-encapsulated and nanoparticle-enhanced thermal energy storage phase change materials, Int. J. Heat Mass Transf. 66 (2013) 575–584.
[43] A. Nokhosteen, S. Sobhansarbandi, Utilizing lattice boltzmann method for heat transfer analysis in solar thermal systems: a review, Sustain. Energy Technol. Assess. 46 (2021), 101264.
[44] E.M. Languri, H.B. Rokni, J. Alvarado, B. Takabi, M. Kong, Heat transfer analysis of microencapsulated phase change material slurry flow in heated helical coils: a numerical and analytical study, Int. J. Heat Mass Transf. 118 (2018) 872–878.
[45] L. Chai, R. Shaukat, L. Wang, H.S. Wang, A review on heat transfer and hydrodynamic characteristics of nano/microencapsulated phase change slurry (N/MPCS) in mini/microchannel heat sinks, Appl. Therm. Eng. 135 (2018) 334–349.
[46] B. Chen, X. Wang, R. Zeng, Y. Zhang, X. Wang, J. Niu, Y. Li, H. Di, An experimental study of convective heat transfer with microencapsulated phase change material suspension: laminar flow in a circular tube under constant heat flux, Exp. Thermal Fluid Sci. 32 (8) (2008) 1638–1646.
[47] E.L. Alisetti, S.K. Roy, Forced convection heat transfer to phase change material slurries in circular ducts, J. Thermophys. Heat Transf. 14 (1) (2000) 115–118.
[48] C.J. Ho, K.H. Lin, S. Rashidi, D. Toghraie, W.M. Yan, Experimental study on thermophysical properties of water-based nanoemulsion of n-eicosane PCM, J. Mol. Liq. 321 (2021), 114760.
[49] M. Ghalambaz, A.J. Chamkha, D. Wen, Natural convective flow and heat transfer of nano-encapsulated phase change materials (NEPCMs) in a cavity, Int. J. Heat Mass Transf. 138 (2019) 738–749.
[50] E. Golab, B. Vahedi, nanoFLuid4Foam (Version 1.0.0) [Computer software]. https://github.com/EhsanGLB/nanoFLuid4Foam, 2023.
[51] M. Abbasi, A.N. Esfahani, E. Golab, O. Golestanian, N. Ashouri, S.M. Sajadi, F. Ghaemi, D. Baleanu, A. Karimipour, Effects of brownian motions and thermophoresis diffusions on the hematocrit and LDL concentration/diameter of pulsatile non-newtonian blood in abdominal aortic aneurysm, J. Non-Newtonian Fluid Mech. 294 (2021), 104576.
[52] S.Y. Motlagh, E. Golab, A.N. Sadr, Two-phase modeling of the free convection of nanofluid inside the inclined porous semi-annulus enclosure, Int. J. Mech. Sci. 164 (2019), 105183.
[53] X. Wang, J. Niu, Y. Li, X. Wang, B. Chen, R. Zeng, Q. Song, Y. Zhang, Flow and heat transfer behaviors of phase change material slurries in a horizontal circular tube, Int. J. Heat Mass Transf. 50 (13–14) (2007) 2480–2491.
[54] Z. Qiu, L. Li, Experimental and numerical investigation of laminar heat transfer of microencapsulated phase change material slurry (MPCMS) in a circular tube with constant heat flux, Sustain. Cities Soc. 52 (2020), 101786.
[55] G. Zhang, G. Cui, B. Dou, Z. Wang, M.A. Goula, An experimental investigation of forced convection heat transfer with novel microencapsulated phase change material slurries in a circular tube under constant heat flux, Energy Convers. Manag. 171 (2018) 699–709.
[56] B. Chen, X. Wang, R. Zeng, Y. Zhang, X. Wang, J. Niu, Y. Li, H. Di, An experimental study of convective heat transfer with microencapsulated phase change material suspension: laminar flow in a circular tube under constant heat flux, Exp. Thermal Fluid Sci. 32 (8) (2008) 1638–1646.
[57] S.Z. Heris, S.G. Etemad, M.N. Esfahany, Experimental investigation of oxide nanofluids laminar flow convective heat transfer, Int. Commun. Heat Mass Transfer 33 (4) (2006) 529–535.